J. Fluid Mech. (1987), *vol.* 175, *pp.* 43–83
Printed in Great Britain

A study of hairpin vortices in a laminar boundary layer. Part 2. Hairpin vortices generated by fluid injection

By M. S. ACARLAR
AT & T Bell Laboratories, Allentown, PA 18015, USA

AND C. R. SMITH
Department of Mechanical Engineering and Mechanics, Lehigh University, Bethlehem, PA 18015, USA

(Received 7 October 1985 and in revised form 27 May 1986)

It has been suggested that hairpin vortices are a major sustaining flow structure involved in the perpetuation of turbulent boundary layers, although their origin within the boundary layer is unclear. One hypothesis is that hairpin structures are formed by the breakdown of the low-speed streak structures which develop adjacent to the surface beneath turbulent boundary layers. To examine this hypothesis, a water-channel study has been done which utilizes injection through surface slots in a flat plate to create artificial low-speed streak-type regions beneath a laminar boundary layer. Under appropriate conditions, these synthesized low-speed streaks develop a three-dimensional, shear-layer instability which breaks down to form a hairpin-vortex street. Employing both flow visualization and anemometry measurements, the characteristics of these hairpin structures and the parameters influencing their generation have been examined. The hairpin streets were determined to develop in a very periodic and repeatable manner within a definite range of flow parameters. Detailed flow patterns obtained using dye and hydrogen bubbles, both individually and collectively, indicate a remarkable similarity with previously observed patterns in the near-wall region of turbulent boundary layers. In addition, the development of the hairpin structures is observed to be quite sensitive to external forcing, as well as exhibiting a tendency for organized development of larger, more complex structures through a pairing-type process. Velocity measurements indicate the initial presence of strong inflexional profiles which evolve rapidly to velocity and turbulence-intensity profiles commensurate with those associated with turbulent boundary layers, but which do not exhibit the marked spreading associated with turbulence.

1. Introduction

The study of boundary-layer turbulence in the last thirty years has clearly demonstrated that the chaotic behaviour referred to as turbulence has a systematic organization. Most researchers share a common belief that a cyclic bursting phenomenon is the predominant mode of turbulence production. The bursting phenomenon can be described as the lift-up, oscillation and subsequent break up of low-speed-streak regions occurring in the near-wall region of turbulent boundary layers. Repeated observations and measurements (Kline *et al.* 1967; Kim, Kline & Reynolds

1971; Laufer & Narayanan 1971; Blackwelder & Kaplan 1976; Achia & Thompson 1976; Lee, Eckelmann & Hanratty 1974; Oldaker & Tiederman 1977; Smith 1978; Blackwelder & Eckelman 1979; Utami & Ueno 1979; Nakagawa & Nezu 1981; and Smith & Metzler 1983) have shown the near-wall region to be the source of the most universally organized and identifiable structures, namely the low-speed streaks, which are observed to be a primary constituent of the turbulent bursts. The other major organized structures and events that are observed in conjunction with bursts are streamwise counter-rotating vortices, sweeps and transverse vortices.

Numerous researchers, employing varying degrees of interpretation and speculation, have hypothesized various models to explain the above cyclic bursting phenomena and the associated structures and events. It appears that the hairpin-vortex models hold a great deal of promise (Brodkey & Wallace 1982; Wallace 1982; Perry & Chong 1982; Smith 1984). According to this model, the counter-rotating streamwise vortices are pictured as the interacting legs of a hairpin stretched by the streamwise mean flow, with the heads of the hairpins construed as the observed transverse vortices. It is suggested that the low-speed streaks are generated and maintained owing to the accumulation of low-momentum fluid between these counter-rotating legs. The burst phenomenon is equated to the sudden lifting of the hairpin vortex and the entrained low-speed streak. The source of the hairpin vortices is hypothesized as a roll-up of the unstable shear layer generated between the lifted-up, low-momentum fluid (low-speed streak) and higher-speed wall-layer fluid. Thus, the hairpin vortices provide a mechanism for (i) lift-up of fluid away from the wall which interacts with the earlier bursts and/or vortical structures (thus creating the break-up stage of the burst event), and (ii) redevelopment and perpetuation of the low-momentum-streak regions following a burst, thus aiding in the formation of new generations of hairpins.

Although hairpin vortex models appear conceptually promising, previous models have several deficiencies; the three most serious of these are as follows.

(i) Although hairpin vortices have been observed in one study to extend throughout the boundary layer (Head & Bandyophadyay 1981) and to occur behind trip wires in transitional boundary layers (Perry, Lim & Teh 1981), their existence in turbulent boundary layers is still not an established fact (Brodkey & Wallace 1982). It is to be noted, however, that recent numerical simulations by Moin & Kim (1985) indicate the clear presence of such hairpin flow structures in a simulated turbulent channnel flow.

(ii) Despite the suggestion that the stretched legs of the hairpins create the low-speed streaks by concentration of low-speed fluid between them, it is unclear how this process can account for the apparent extreme length and persistence of streaks (Oldaker & Tiederman 1977; Blackwelder & Eckelmann 1979). Although Smith & Metzler (1983) and Smith (1984) suggest a conceptual mechanism illustrating how hairpins reinforce, perpetuate and redevelop low-speed streaks, the role of hairpins in these events have not been physically demonstrated.

(iii) The burst sequence has been described (Kim *et al.* 1971; Kline 1978) to be the lift-up of a streak from the wall, followed by a violent oscillation and break-up of the low-speed streak. Although Offen & Kline (1975), and Wallace (1982) suggest the importance of hairpins in the bursting sequence, their suggestions are only interpretations and speculations. Head & Bandyophadyay (1981) and Perry & Chong (1982) discuss the formation of hairpins as necessary for the development of turbulent boundary layers, but do not relate them to the cyclic turbulence processes (i.e. bursts,

ejections, sweeps) or the low-speed streaks. Thus, the role of hairpin vortices in the cyclic turbulence processes has not been established.

A major stumbling block in resolving many of the questions or deficiencies associated with hairpin-vortex models of boundary-layer turbulence is our lack of understanding of the actual behaviour of hairpin-shaped vortices. Until recently, no study has been done to directly assess their characteristics and behaviour. However, in a companion paper to the study described here (Acarlar & Smith 1987), a detailed empirical investigation of hairpin vortices generated by the shedding of hemisphere proturberances is reported. Acarlar & Smith not only establish many of the behavioural aspects of hairpin vortices, but also demonstrate that hairpin vortices generated in an otherwise laminar environment give rise to visualization patterns and velocity statistics that are essentially the same as those obtained in turbulent boundary layers.

Although the Acarlar & Smith study strongly suggests that hairpin vortices do exist in turbulent boundary layers, it does not address the question of the origin of the hairpins. It is suggested by Kim *et al.* (1971), Hinze (1975), and Smith (1984) that local near-wall inflexional profiles give rise directly to hairpin-vortex generation. Furthermore, Wallace (1982) has suggested that local pressure-field fluctuations distort and destabilize shear layers diffusing from the wall region, causing hairpin vortices to form. Thus, it is expected that the artificial creation of an inflexional profile would yield flow structures and behaviour that are more similar to the events occurring within a turbulent boundary layer than the flow structures generated by solid proturberances.

The present paper presents a study of the flow structure and behaviour resulting from the creation of a local inflexional velocity profile within an initially subcritical laminar boundary layer via continuous injection through a thin streamwise slot. This injection of new fluid into the boundary layer is intended to simulate the development of a low-speed streak in the near-wall region of a turbulent boundary layer. Because the injected fluid has no initial streamwise momentum, it creates an elongated, locally retarded flow region just above the wall. This yields a velocity profile (u) with $\partial u/\partial y = 0$ at a point above the wall, which Van Dommelen (1981) has demonstrated as a necessary condition for the breakdown of a viscous, wall-region flow. A velocity profile with a point of vanishing $\partial u/\partial y$ must also contain an inflexion point, which is of course unstable and, as will be illustrated in this paper, results in a shear-layer breakdown into a series of hairpin vortices similar to those produced by hemisphere shedding and reported on in Part 1 of this work (Acarlar & Smith 1987).

Generally, the objectives of the present study were to:

(i) Examine the shedding conditions and characteristics of the hairpin vortices generated by the synthetic streak roll-up.

(ii) Establish the developmental behaviour of these hairpin vortices throughout their evolution.

(iii) Examine the effects of the vortices on the immediate surrounding regions, the subsequent structures they generate, and their effect on the general stability characteristics of an initially laminar boundary layer.

(iv) Examine the role of outer-layer disturbances on the synthetic low-speed-streak behaviour and establish the potential role that outer-layer structures might play in the streak break-up process within turbulent boundary layers.

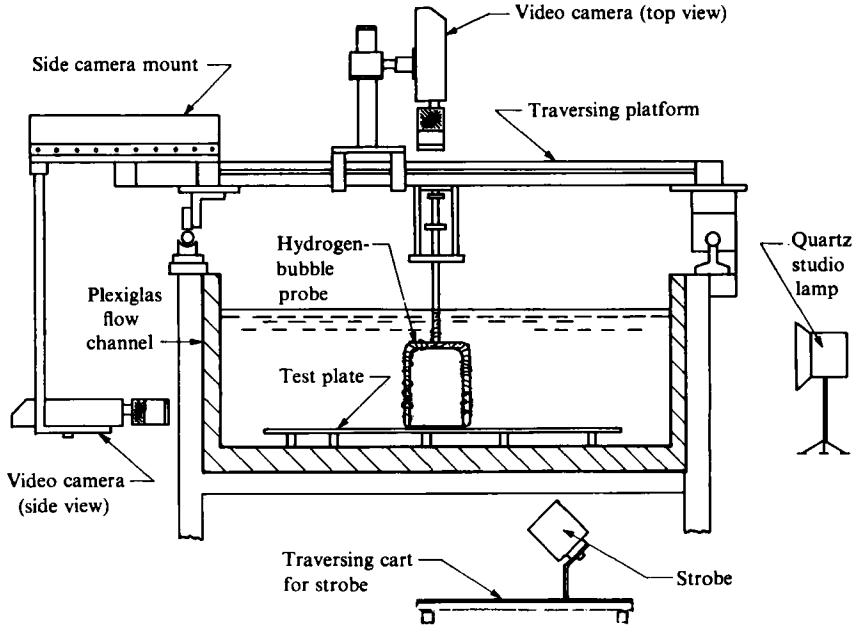

FIGURE 1. End-view schematic of water-channel facility (flow is out of page).

2. Special equipment and techniques

The present studies were performed in a free-surface water-channel facility with a 5 m working section, 0.9 m wide and 0.4 m deep, as described in Smith & Metzler (1983). A general schematic of the facility and the associated equipment is shown in figure 1.

Hairpin vortices are generated by the unstable interaction of an artificial low-speed region with a subcritical laminar boundary layer. This artificial low-speed region is introduced by injection of fluid through a streamwise slot beneath a laminar boundary layer. A 9.5 mm thick Plexiglas flat plate, 0.85 m long and 0.5 m wide, with a 5:1 elliptical leading edge was utilized as a test section. The plate was supported 10 cm above the channel surface by four adjustable legs to allow controlled development of a laminar boundary layer and to prevent interference by channel-wall boundary layers. Uniformity of the flow above and below the plate was checked and assured using hydrogen-bubble visualization.

As shown in figure 2, a streamwise slot, 1 mm in width and 63.5 mm in length, is used to generate the synthetic low-speed streak via continuous uniform injection of water normal to the plate surface. A half-cylinder reservoir located beneath the streamwise slot assures uniform injection. An external reservoir supplies the water for the streamwise-slot injection. The water used in the reservoir is taken from the channel to assure fluid uniformity. A micro-rotameter monitors the injection rate. A dye reservoir is connected by a T-junction to the water injection line to allow introduction of dye into the low-speed injection fluid.

Three spanwise dye slots were utilized to introduce dye both upstream and downstream of the synthetic streak as shown in figure 2. These dye slots were located 10 cm upstream, 10 cm downstream, and 24 cm downstream of the streamwise slot to allow visualization of the different regions of the wake and near-wall structures.

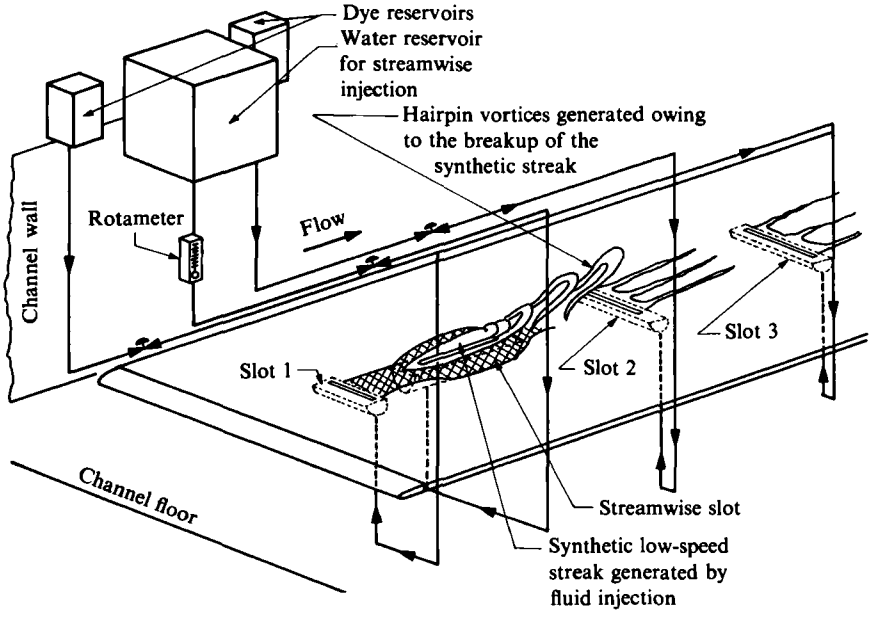

FIGURE 2. Schematic of streamwise slot and dye injection technique.

In order to prevent possible de-stabilization of the boundary layer, dye injection from the spanwise slots was kept below the critical values suggested by Oldaker & Tiederman (1977); stability of the initial laminar boundary layer with spanwise slot injection was confirmed by both near-wall hydrogen-bubble visualization and hot-film-anemometry measurements, which indicated uniform, steady behaviour up to the maximum injection rate employed.

The hairpin vortices and associated secondary flow structures (i.e. low-speed concentrations, secondary vortices, ejections, and burst-like events) were visualized both by marking the hairpins with dye at the point of generation and by bleeding-in different colours of dye upstream and downstream of the generation point. An overhead traverse platform with a variable-speed drive was extensively utilized to visualize the development and evolution of the hairpin vortices from a Lagrangian reference frame. Figure 1 illustrates the method for mounting two video cameras on the upper traversing platform to provide side and top views. Hot-film and hydrogen-bubble-wire probes were also mounted on the upper platform; the lower platform was primarily used for lighting purposes.

Both hydrogen-bubble-wire and dye-visualization techniques were extensively employed to study the hairpin vortices and their evolution. A technique that utilized a combination of these two techniques proved to be very useful, despite the difficulties in developing appropriate lighting and background. Utilizing this combined visualization technique, hairpin vortices and the visualization patterns created by their presence could be observed simultaneously.

The flow patterns were visualized using bubble-wire probes which allow a 25 μm diameter platinum wire, 20 cm in length, to be located parallel to (horizontal hydrogen-bubble-wire probe) or normal to (vertical hydrogen-bubble-wire probe) the flat plate and transverse to the flow direction. Using these probes, mounted on the traversing platform, lines and sheets of hydrogen bubbles could be introduced in any

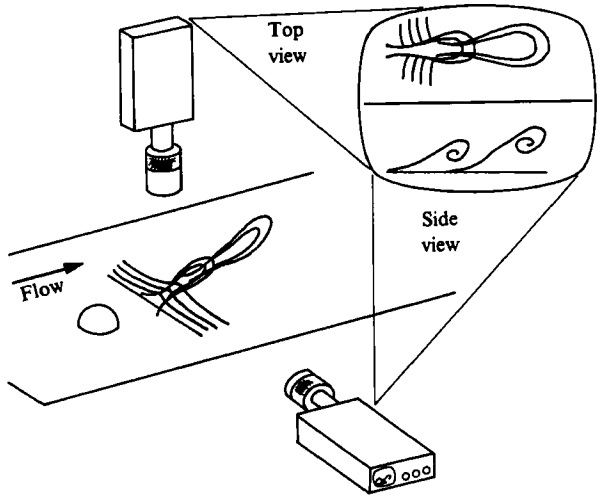

FIGURE 3. Schematic for split-screen viewing (top–side view).

location and orientation relative to the flat-plate surface and hairpin-vortex orientation.

The advantage of the hydrogen-bubble method is that it reveals the local active behaviour and carries a minimum of flow history, unlike dye visualization. In addition, the details of the flow field can be visualized, whereas with conventional dye visualization only the 'skin' or the outer borders of the structures can generally be visualized. (Note that methods employing laser-light sheets can reveal interior details, but the dye patterns still are reflective of the history of the dye in the flow field, not the local behaviour.) The hydrogen-bubble method is also more useful for obtaining quantitative information by geometric measurement and time-of-flight techniques (see Lu & Smith 1985).

The viewing and recording system employed in the studies is a two-camera, high-speed video system (manufactured by Video Logic Co.) which incorporates synchronized strobe lights to provide 120 frame/s with effective exposure times of 10^{-4} s. A split-screen capability allows two different fields-of-view to be simultaneously displayed and recorded. Figure 3 is a schematic of the camera set-up for one of the split-screen viewing techniques employed. The video system is described in greater detail by Smith (1982) for various applications.

The lighting techniques used for both the dye and hydrogen-bubble visualization were quite standard, and are discussed in detail elsewhere (Acarlar & Smith 1984). The lighting and background employed for the *combined* use of dye and hydrogen bubbles was much more difficult, owing to the opposing background and lighting requirements of each individual visualization technique. Dye visualization generally requires a light background and back-lighting techniques, whereas hydrogen-bubble visualization requires a dark background and oblique, refractive lighting. After trying various colour backgrounds and lighting techniques it was determined that a gold plastic background (as suggested by Offen & Kline 1974) without backlighting gives the best results.

End views of the generation and evolution of hairpin vortices were visualized using a horizontal (spanwise) hydrogen-bubble wire. Use of dye visualization proved unsatisfactory owing to the dark background experienced when looking upstream

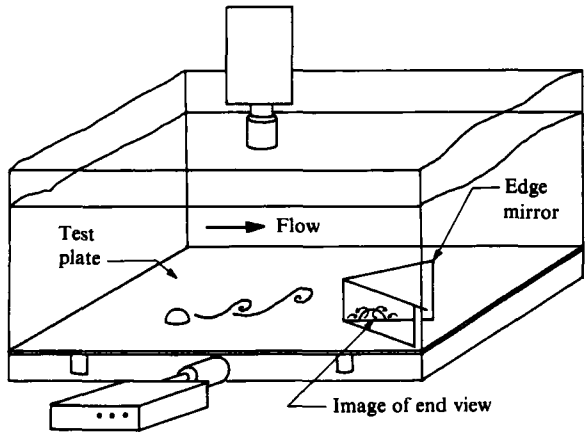

FIGURE 4. Schematic of top–end-view visualization.

from end view. A schematic illustrating the technique employed for top–end visualizations is shown in figure 4. A front-silvered wedge mirror (to assure the symmetry of the flow field) was located 30 cm downstream of the hairpin generation location. The apex angle of the mirror was optimized at 30°, which was found to minimize blockage effects while providing a sufficient reflection angle. To assure that the flow is not affected by the presence of the mirror, the flow field was visualized at a series of locations upstream of the mirror to examine qualitative changes; it was established that the mirror imparts no changes in the regions of interest. To assure alignment and equal magnification of the two simultaneous views, a fixed-geometry calibration insert of 1 mm thick Plexiglas with a carefully scribed rectangular pattern was used.

To facilitate the determination of local motion, single-realization bubble lines were generally used for the end-view studies with the frequency and duration of the hydrogen-bubble lines synchronized with the frequency of hairpin generation. This technique proved to be the most useful for end-view visualization of hairpin vortices, allowing the marking of a single hairpin vortex with only a single bubble line. Since in the end-view visualization the bubble lines move along the viewing direction of the camera, the depth of field was maximized by appropriate lighting techniques to assure that the bubble line would remain in focus. Lighting was generally accomplished using the 1000 watt strobe directed downstream at an angle of $\approx 40°$ to the line-of-sight of the camera.

Mean-velocity and turbulence-intensity profiles were obtained at several downstream locations in the wake using a DISA 55D01 constant-temperature hot-film anemometer, DISA 55M25 linearizer, a TSI-1076 true RMS voltmeter, and a DEC PDP 11/23 Minc data-acquisition computer. Mean and fluctuating velocity in the streamwise direction were measured using DISA 55 R11 or 55 R15 hot-film probes mounted with the sensor parallel to the test-section walls. The linearization procedure involved towing the probe through the quiescent channel over a range of velocities. The linearization technique utilized is described in Acarlar & Smith (1984).

Time averages over at least 300 cycles of hairpin generation were used to establish mean data at each measurement point. Lengthy averaging times were employed to ensure stable average measurements. The measurement points comprising each profile (both mean velocity and turbulence intensity) were taken sufficiently close

together such that variations from point to point did not exceed 10%. The approximate total time for measurement of each profile was 4–8 h. Over this time period, some drift would often be experienced due to dirt build-up on the probe sensor and/or water temperature variations. To correct for voltage drift, the calibrated velocity output was corrected using a simple linear correction technique suggested by the work of Morrow & Kline (1974). A presentation, discussion, and verification of this technique is presented in Bacher & Smith (1985).

Vortex-shedding frequencies were determined employing hot-film-anemometry measurements and the data-acquisition system. The downstream location and the height of the hot-film probe were adjusted such that it was only affected by the passage of the head of the hairpin vortices. Hot-film data were input to the minicomputer and stored on disk. Shedding frequencies were then determined using standard fast-Fourier-transform techniques. The shedding frequencies were checked by simultaneous display of the anemometer signal on a storage oscilloscope.

3. Initial observations

Figure 5(*a*) is a schematic illustration of the process of hairpin-vortex generation due to the break-up of a synthetic low-speed streak created by continuous and uniform injection through the streamwise slot. The low-speed-fluid region, which is artificially generated near the wall, is called a 'synthetic low-speed' streak because of its extreme visual similarity to the low-speed streaks observed by Kline *et al.* (1967) and Smith & Metzler (1983) in the wall region of turbulent boundary layers. When the injection rate is raised above a critical value, the synthetic low-speed region becomes unstable, initiating an oscillation which breaks down into horseshoe-type vortices. These vortices are carried downstream by the mean flow and undergo stretching by the wall shear layer. This stretching process causes the horseshoe-shaped vortices to elongate into hairpin-type vortices. As the heads and legs of the vortices lift-up from the surface owing to mutual induction, they are further stretched, which increases the induced velocity effects and causes the further migration of the stretched legs away from the wall. The trailing portion of the legs which remain near the wall create local lateral pressure gradients which cause the accumulation, concentration, and lift-up of low-momentum fluid between the counter-rotating legs (see Ersoy & Walker 1985, for discussion of this mechanism). The consequences of this concentration and lift-up process on the already existing hairpin vortices will be discussed later. Figure 5(*b*) is a combined top–side dye visualization of the hairpin-vortex formation process described above and illustrated schematically in figure 5(*a*). The oscillation and initiation of the vortex roll-up can be clearly observed in the side view.

Figure 6(*a*) is a side-view visualization of hairpin vortices at $x/\theta = 36$ downstream location (θ is the momentum thickness of the impinging laminar boundary layer, x the downstream distance from the trailing edge of the streamwise slot); figure 6(*b*) is a vertical hydrogen-bubble-wire visualization of essentially the same structures on the symmetry plane, illustrating the rotational behaviour within the tip of the hairpin.

Figure 7 is a schematic illustrating the break-up of the low-speed stream to form hairpin vortices. The impinging boundary-layer flow is deflected by the presence of the injected fluid, passing over and around the lower-speed region; the result is the contouring of the synthetic streak by the impinging flow which causes the synthetic streaks to assume a streamlined appearance, as shown in figure 7.

Figure 8 is a top-view dye visualization of the flow in the vicinity of a synthetic

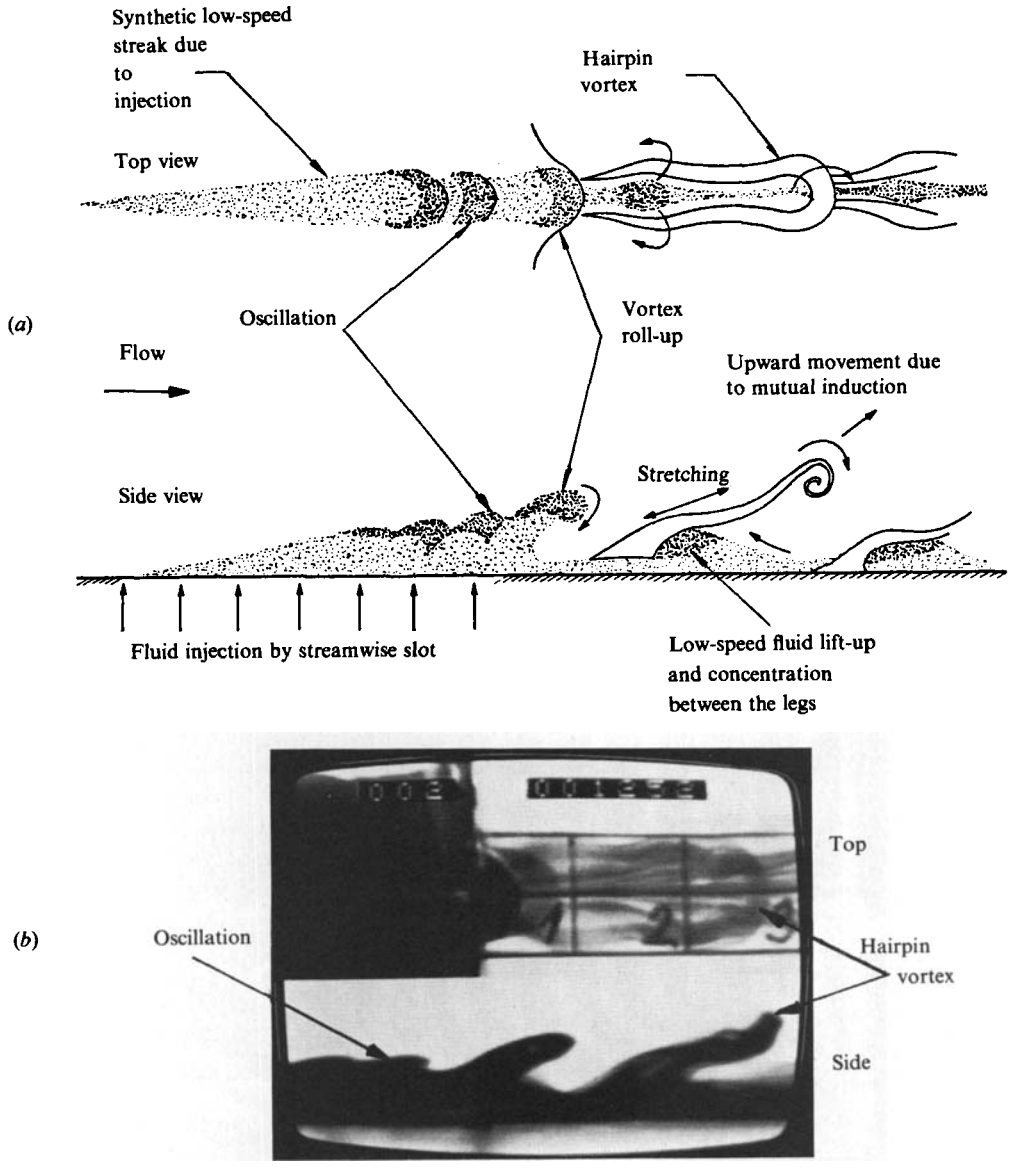

FIGURE 5. (*a*) Schematic showing the generation of the hairpin vortices due to the roll-up of the low-speed region created by injection. (*b*) Top–side view of the generated hairpin vortices.

streak. Dye is introduced into the boundary layer via the upstream spanwise slot (see figure 2). Note that figure 8 was obtained by injecting clear water through the streamwise slot; this allows visualization of the behaviour of the surface fluid in the vicinity of the synthetic low-speed streak and the hairpin-generation region. The lift-up of low-momentum fluid due to effects imposed by the counter-rotating legs of the hairpin vortices in proximity to the wall is visualized by the dark concentration of dye downstream of the 5 cm mark line (marked as 1 in figure 8).

Note that although the fluid injection process does not generate a stagnation-point flow, as was observed for the hemisphere shedding studied in Part 1 of this work

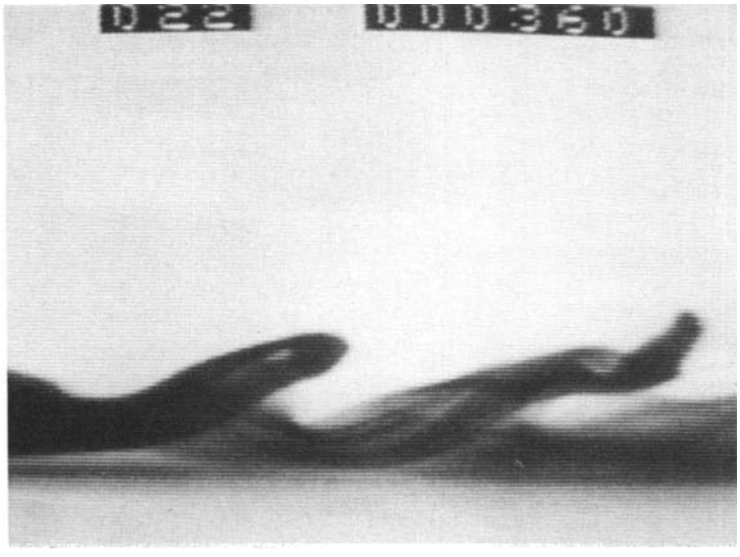

(a)

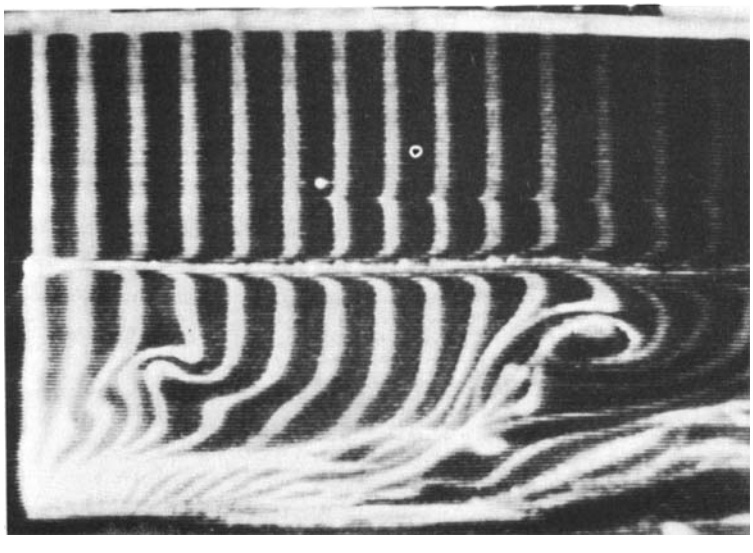

(b)

FIGURE 6. Side-view of hairpin vortices at $x/\theta = 36$, $Re_\theta = 135$. (a) Dye patterns. (b) Hydrogen-bubble-line patterns.

(Acarlar & Smith 1987), a secondary-vortex flow structure was observed to develop which is similar in configuration and behaviour to the horseshoe-type vortex observed to form at bluff body/end wall junctures. Figure 7 illustrates the location of these secondary streamwise vortices which form *outboard* of the counter-rotating legs of the hairpin vortices, and extend well downstream of the injection slot. In general, these secondary vortical structures were weaker than the typical horseshoe-type vortex, and appeared to strengthen and develop with downstream distance. The presence of these vortex structures is revealed in figure 8 by the development of two dye

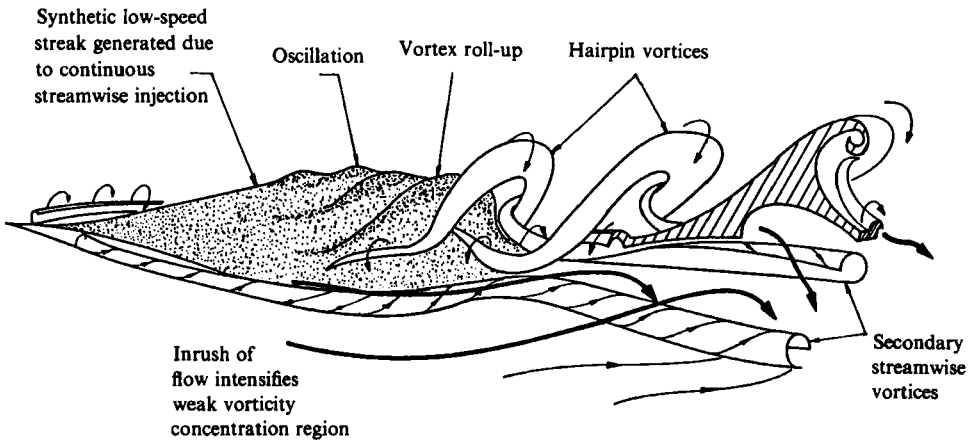

FIGURE 7. Schematic of break-up of a synthetic low-speed streak generating hairpin vortices. Secondary streamwise vortical structures are generated owing to inrush of fluid.

concentrations (one is marked as 3) which appear laterally to either side of the dark dye concentration created by the counter-rotating legs of the hairpin vortices (marked as 1). The presence of these outboard vortical structures will be illustrated in § 5 (particularly in figure 13).

4. Frequency characteristics

The dependence of the frequency of hairpin generation on free-stream velocity and injection rate was established using power-spectral analysis of hot-film-anemometry measurements, as described in § 2. The periodicity of the roll-up and generation of hairpin vortices was examined for four different streamwise slot geometries. The frequency characteristics are presented here for only one slot geometry; for information on the characteristics produced by the other slots see Acarlar & Smith (1984). Figure 9 shows the roll-up frequency versus free-stream velocity characteristics obtained with a 63.5×1 mm streamwise slot for a series of injection velocities. Figure 9 indicates that the hairpin-vortex generation frequency increases with both the free-stream and the injection velocity. For a fixed injection velocity, an empirical regression analysis indicated that the roll-up frequency of hairpins can be approximated as

$$f = K_{V_w} V_w U_\infty^{1.25}, \tag{4.1}$$

where f = roll-up frequency (frequency of hairpin generation), K_{V_w} = a constant for each slot injection velocity, V_w = injection velocity, U_∞ = free-stream velocity.

Figure 10 shows the data of figure 9 replotted in a dimensionless form of f^* versus Re_{δ^*} ($f^* = f\delta^*/U_\infty$, $Re_{\delta^*} = U_\infty \delta^*/\nu$, where δ^* is the displacement thickness of the impinging boundary layer at the beginning of the slot). Re_{V_w} is based on the injection velocity, V_w; width of the slot, w; and kinematic viscosity, ν. From figure 10 one can observe that increasing Re_{δ^*} results in a corresponding decrease in f^*. Increasing Re_{V_w} (an increase in V_w with constant slot width) causes an upward shift in the curve. Note that the extent of the data in Re_{δ^*} is the extent of the region over which stable hairpin generation would occur; below $Re_{\delta^*} \approx 200$ vortex shedding did not occur and above $Re_{\delta^*} \approx 550$ the shedding process became unstable (as one might suspect, since

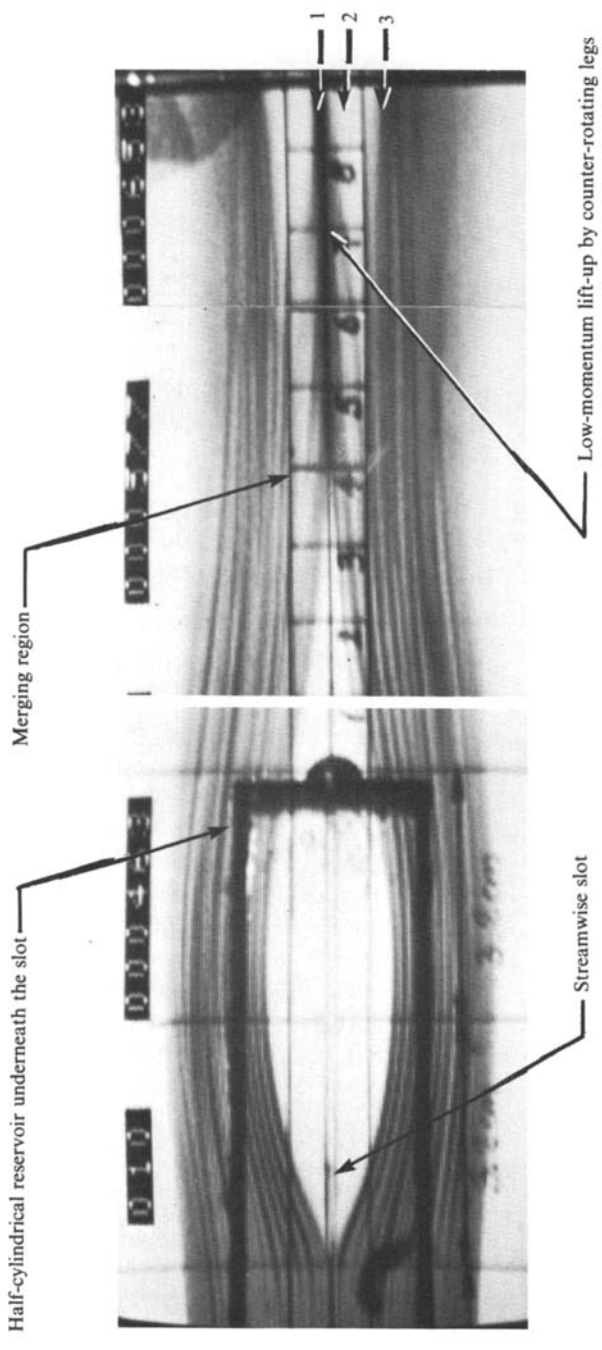

FIGURE 8. Top-view dye visualization of the flow in the vicinity of the synthetic streak. Dye is introduced into the boundary layer upstream of the streamwise slot. Only clear water is injected through the streamwise slot. $Re_\theta = 135$.

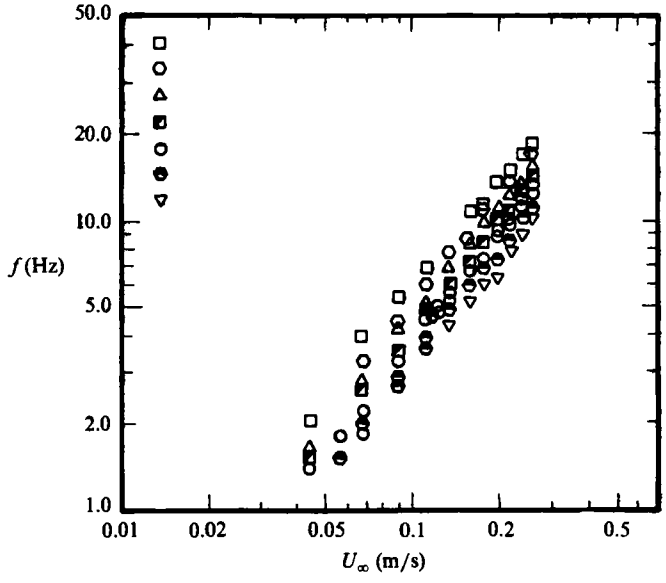

FIGURE 9. Roll-up characteristics for a 63.5 mm × 1 mm streamwise slot. $f = K_{V_w} V_w U^{1.25}$. ▽, V_w = 1.05 cm/s; ◓, 1.31 cm/s; ○, 1.57 cm/s; ◩, 1.84 cm/s; △, 2.10 cm/s; ⬡, 2.36 cm/s; □, 2.62 cm/s.

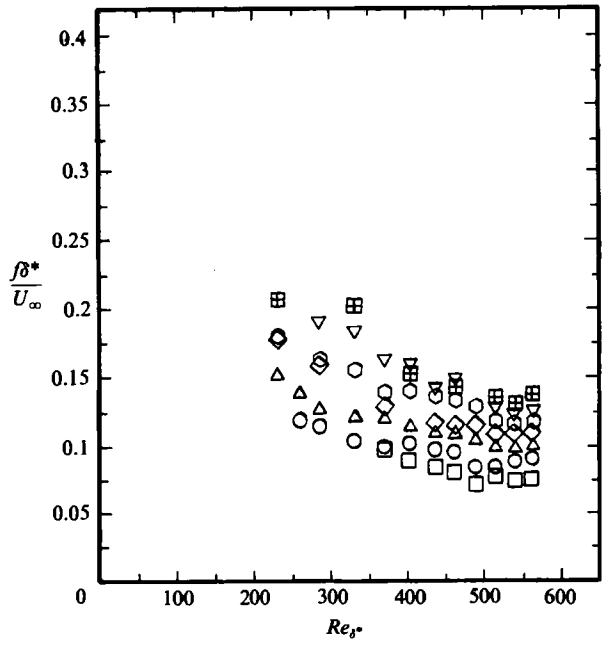

FIGURE 10. Non-dimensional frequency f^* versus Re_{δ^*} for data shown in figure 9. Symbols correspond to different injection velocities. $Re_{\delta^*} = U_{\infty\delta^*}/\nu$, $Re_{V_w} = wV_w/\nu$. □, Re_{V_w} = 11.3; ○, 14.1; △, 17.0; ◇ 19.8; ⬡, 22.6; ▽, 25.4; ⊞, 28.3.

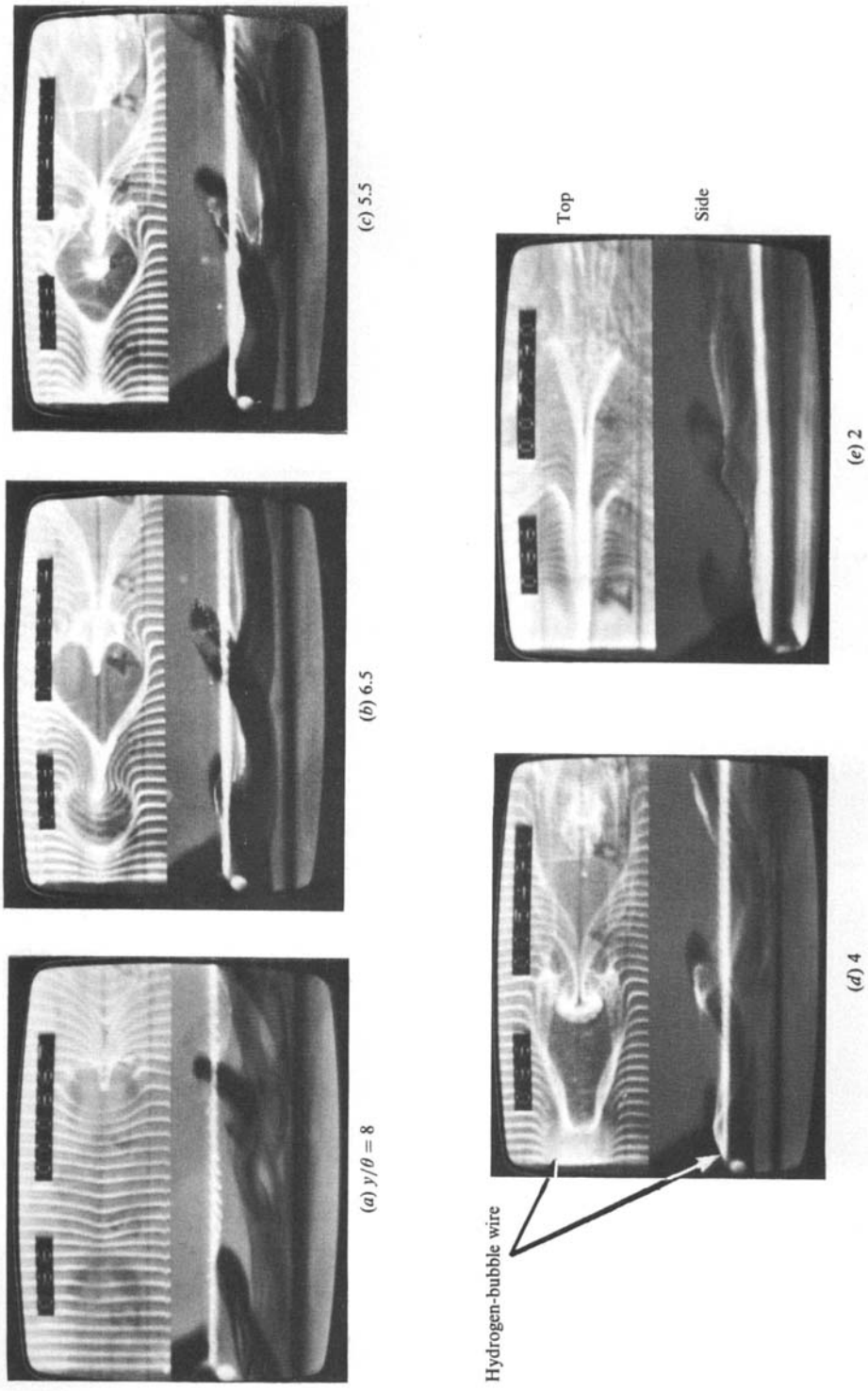

FIGURE 11. Top–side view patterns created by hairpin vortices with bubble-wire at $x/\theta = 12$ from the end of the streamwise slot. Note use of combined hydrogen bubbles and dye injection through slot. $Re_\theta = 135$, $Re_{V_w} = 17$, $V_w/U_\infty = 0.150$.

$Re_{\delta^*_{crit}} \approx 520$ for a Blasius boundary layer). Essentially, the results indicate that stable hairpin-vortex generation can take place in a subcritical, laminar boundary layer. Stable hairpin generation was observed to occur for essentially the same range of Re_{δ^*} for the other three slot geometries examined (both shorter and wider slots), which otherwise demonstrate some moderate f^* variations with geometry.

5. Flow patterns

This section presents and interprets a series of combined top–side view and end-view visualizations obtained by using a combination of dye and hydrogen-bubble flow visualization. The intent is to illustrate the evolution of the hairpin vortices following their generation by the breakdown of a synthetic streak.

Figure 11 is a combined top–side view with dye and hydrogen bubbles obtained at a downstream location of $x/\theta = 12$ (where θ is the momentum thickness at the point of hairpin roll-up). Introduction of dye through the streamwise slot allows the hairpin vortices to be directly visualized in conjunction with the flow field induced by the hairpins, which is illustrated by hydrogen-bubble time-lines from a horizontal (spanwise) bubble wire. Figure 11 illustrates the effect of variations in bubble-wire height on the visualized patterns. As the hydrogen-bubble wire is lowered towards the plate (figure 11*a–e*) the bubble-line patterns reflect the presence of the hairpin tip (figure 11*a*), the head (figure 11*b*), the counter-rotating legs (figure 11*c*, *d*), and very near the wall (figure 11*e*) a streak-like low-speed concentration between the counter-rotating legs.

One can note the similarity between the low-speed streaks of the turbulent boundary layer, an example of which is shown in figure 17(*d*), and the elongated low-speed region visualized near the wall in figure 11(*e*). Detailed study of numerous video sequences of the behaviour of these low-speed regions indicated that these low-speed concentrations first lift-up, begin to oscillate, and then are rapidly carried away from the wall and downstream by the hairpin vortex. In previous visualization studies of turbulent boundary layers by Kim *et al.* (1971) and Offen & Kline (1975), the lift-up, oscillation, and breakdown of the low-speed streaks was described and claimed to be the sequence associated with the bursting process in turbulent boundary layers. Figure 11(*e*) clearly illustrates a lift-up and oscillation phase of the low-speed region; the similarity with the description of turbulence-related bursting is very suggestive, and is addressed further in §7.

Figure 12 is an end-view hydrogen-bubble visualization of a hairpin vortex. The formations marked B are the secondary streamwise vortices shown in the schematic of figure 7. A schematic, shown in figure 12 (*a*), illustrates the process of intensification of these secondary vortical structures due to the velocity gradients generated by inrushing flow. Fluid that is induced down toward the wall outboard of the counter-rotating legs of the hairpin vortices and an inrush of fluid due to continuity (to replace fluid that is lifted-up from the wall between the counter-rotating legs) combine to cause the formation of saddle points on the wall to either side of the hairpin vortex. These saddle points are marked as S in the schematic of figure 12(*a*). Secondary streamwise vortices developing outboard of these saddle points are generated with an opposite sense of rotation to the adjacent hairpin leg. Since the bubble wire in figure 12(*a*) is located above the centre of the core of these outboard vortical structures, the existence of these structures is manifested as a downward movement and roll-up of the bubble lines. Note that the location of the bubble wire in figure 12(*a*) is 3 cm downstream of the streamwise slot, at the beginning of the

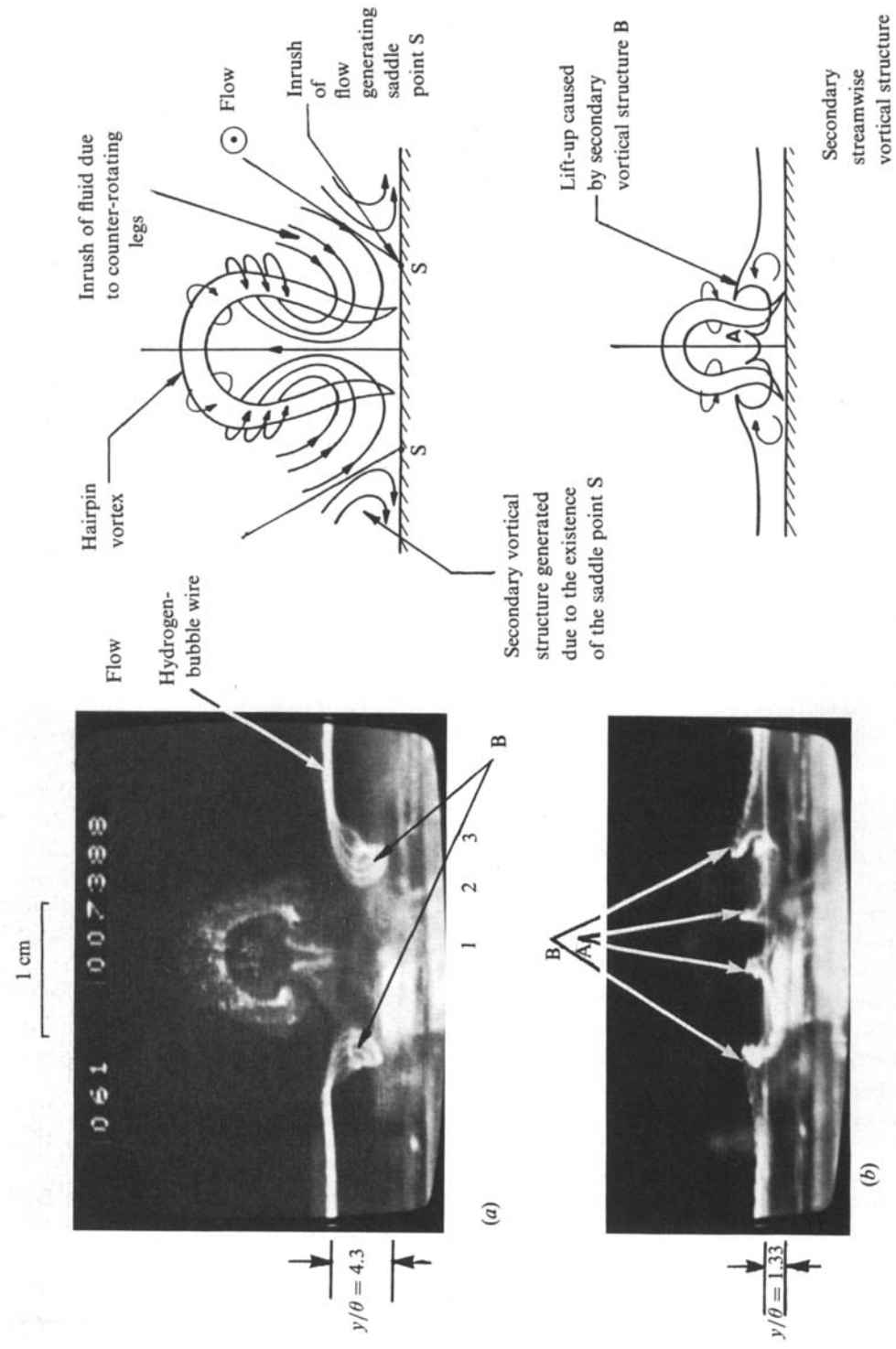

FIGURE 12. End-view hydrogen-bubble-line patterns and corresponding schematics. $Re_\theta = 135$, $Re_{V_w} = 17$, $V_w/U_\infty = 0.150$. (*a*) Hairpin vortex, $x/\theta = 24$; (*b*) Low-momentum lift-ups, $x/\theta = 40$.

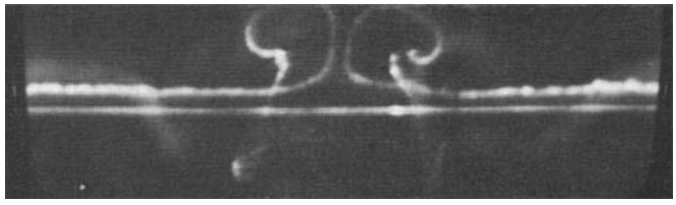

FIGURE 13. End-view visualization of the counter-rotating legs of a hairpin vortex. $x/\theta = 32$, $Re_\theta = 135$, $Re_{V_w} = 17$, $V_w/U_\infty = 0.150$.

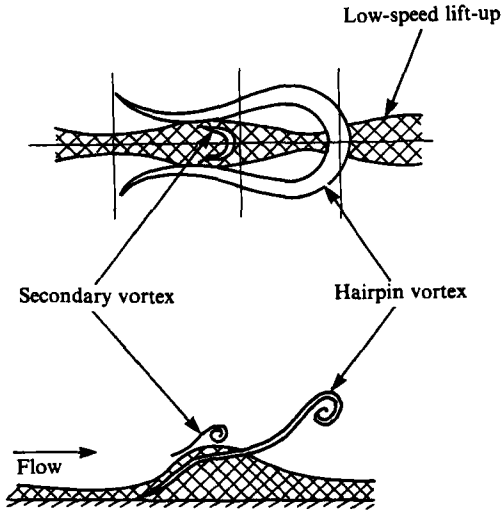

FIGURE 14. Generation of secondary vortices due to the interaction between the lifted-up low-momentum fluid and higher-speed outer flow.

merging region indicated on figure 8. Downstream of this merging region there is an inrush of fluid towards the wall as shown in figure 7. Locating the bubble-wire 5 cm downstream and moving the wire closer to the wall yields the bubble-line pattern shown in figure 12(*b*). In this figure, the fluid lift-ups caused by the counter-rotating legs of the hairpins are marked as A. Since the bubble wire is now below the centre of the cores of the secondary streamwise vortices, their presence is manifested by additional lift-ups of the hydrogen bubbles in this region. These lift-ups are denoted by points B in figure 12(*b*).

Figure 13 is another end-view obtained by the generation of a single hydrogen-bubble line which clearly reveals the effects of the legs of the hairpin vortices. Using this technique, the rotation of the counter-rotating legs is visualized as a double-sided roll-up illustrating a 'mushroom'-type pattern characteristic of this counter-rotating behaviour.

6. Secondary instabilities

Figure 14 is a combined top- and side-view schematic illustrating the development of a secondary vortex in proximity to the primary hairpin vortex structure. This schematic is an idealization developed from the detailed observation of a series of dual-view visualizations of hairpins approximately $x/\theta = 40$–60 downstream of the

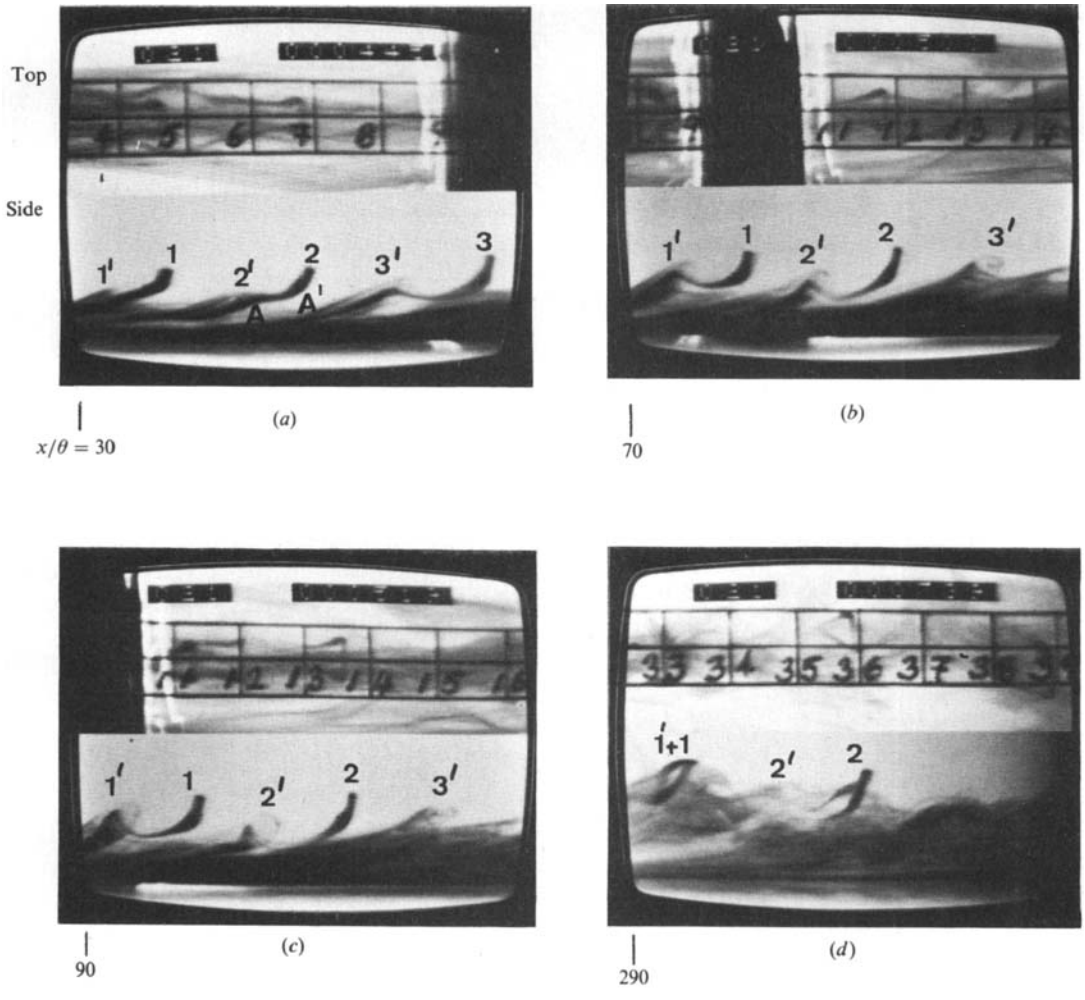

FIGURE 15. Generation of secondary vortices on the plane of symmetry. $Re_\theta = 150$, $Re_{V_w} = 17$, $V_w/U_\infty = 0.126$.

injection slot. As are indicated in this figure, secondary vortical structures appear to be generated owing to the roll-up of the high-shear layer which develops between the lifted-up, low-momentum, wall-layer fluid and the higher-momentum, outer boundary-layer flow. This secondary vortex generation was a common occurrence, appearing to occur to a greater or lesser degree for all cases examined.

In order to study the generation/evolution of these secondary vortical structures and their effect on the original hairpins, the hairpin development was observed in a convected reference frame using the video viewing cameras mounted on the traversing platform. The convection velocities of the hairpin vortices† and the translating platform were matched to allow the recording of the Lagrangian development of the hairpin structures. Figure 15 is a combined top–side visualization of the generation and evolution of these secondary vortices. In figure 15(*a*), the

† Note that the convection velocities initially increase, but reach an approximately terminal velocity fairly rapidly within the field-of-view.

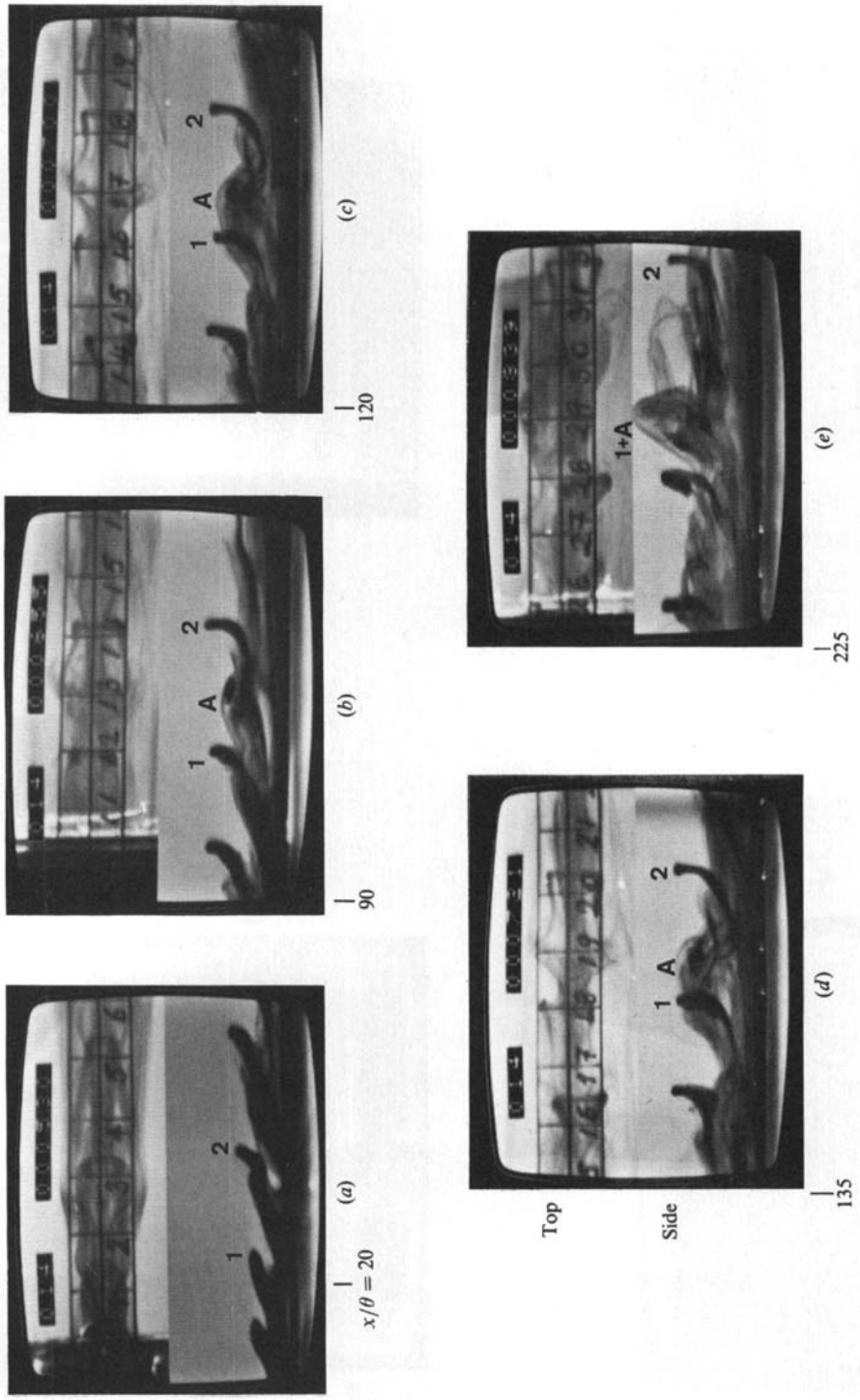

FIGURE 16. Development, interaction and breakdown of a secondary vortex. Obtained by mounting the cameras on the moving platform and matching the velocities. $Re_\theta = 150$, $Re_{V_w} = 17$, $V_w/U_\infty = 0.126$.

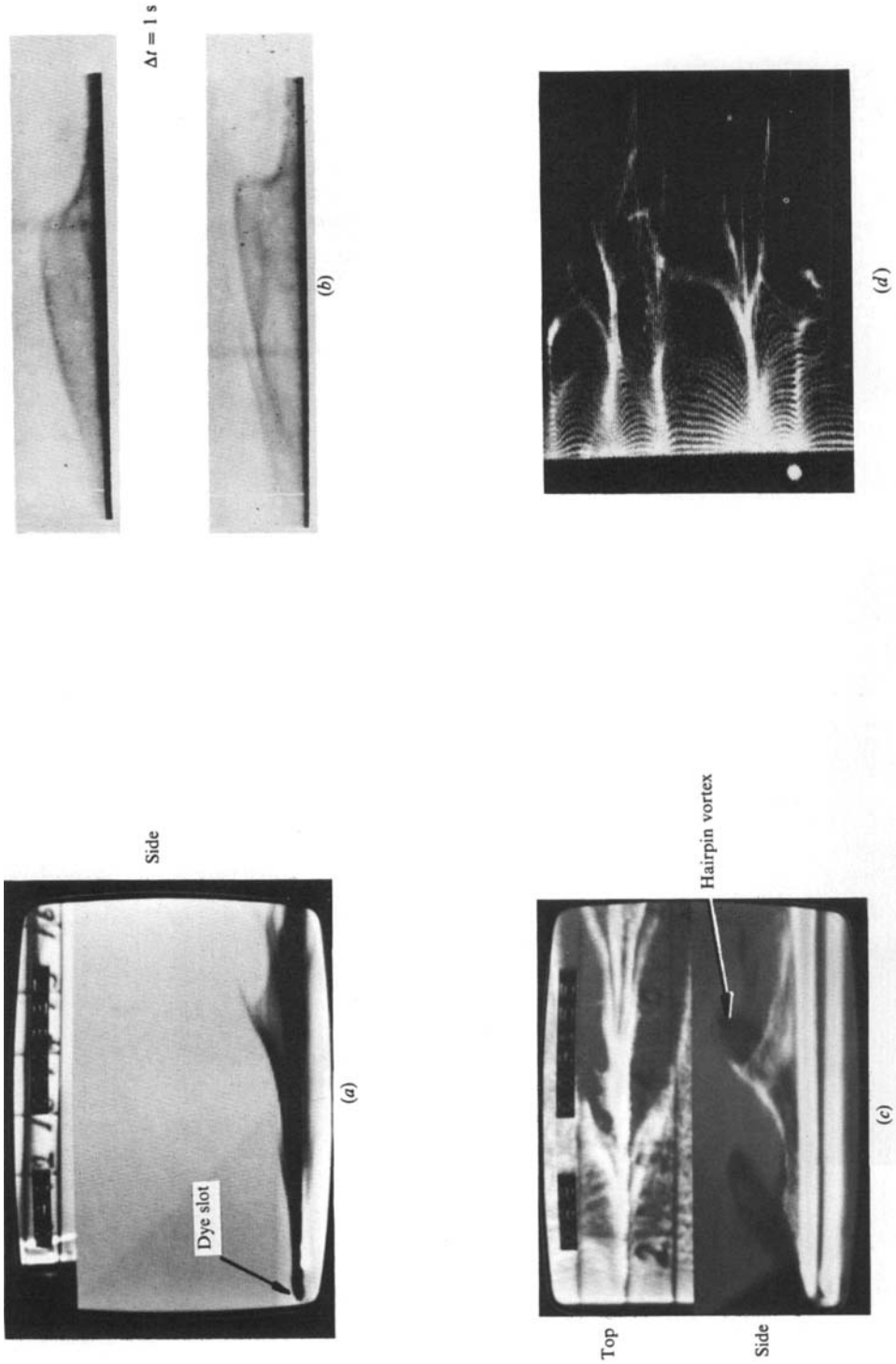

FIGURE 17. Near-wall patterns. (*a*) Lift-up and break-up process of the low-speed concentration created in the wake of the synthetic low-speed streak. (*b*) Dye streak break-up observed in a turbulent boundary layer (Runstadler *et al.* 1963). (*c*) Hydrogen-bubble-line patterns of lift-up. (*d*) Turbulent boundary-layer low-speed streaks.

original hairpins are indicated as 1, 2, and 3. The shear layers which develop between the lifted-up low-momentum fluid and the higher-speed outer boundary layer flow are indicated as 1′, 2′ and 3′ respectively. Note that the shear layer just upstream of hairpin vortex 3 has already begun to roll-up and form a vortical structure 3′. Point A marks the beginning of the region where the counter-rotating legs of the original hairpins are weakened because of mutual vorticity-cancellation effects (see a discussion of this process in § 9); this creates a kinked region (marked AA′ for hairpin 2) which is characteristic of the observed deformation of a hairpin vortex. As the vortices are followed downstream, all three of these shear layers evolve and roll-up, forming the vortical structures marked 1′, 2′, and 3′ in figure 15 (*b*) By $x/\theta = 90$ (figure 15*c*), these secondary vortices evolve further and assume the shape of horseshoe or hairpin vortices. As these secondary vortices evolve, they begin to interact and agglomerate with the original hairpin vortices. The result is the development of complicated large-scale structures which are observed to move suddenly away from the wall in a somewhat chaotic fashion. This stage of the evolution process for the hairpin vortex 1 and secondary vortex 1′ is shown in figure 15 (*d*).

Often the secondary vortex may interact with the trailing hairpin rather than the preceding hairpin vortex; such a development is shown in figure 16. In figure 16 (*a*), $x/\theta = 20$, two hairpin vortices, labelled as 1 and 2 are followed. At $x/\theta = 90$ (figure 16*b*) a secondary vortex (labelled A) begins to develop between hairpins 1 and 2. By $x/\theta = 150$ (figure 16*d*) this secondary vortex (A) has begun to interact by apparent coalescence with the trailing hairpin, 1. The result is again an eruptive and rapid ejection away from the surface as shown in figure 16 (*e*).

7. Near-wall structure

Figure 17 is shown to emphasize the similarity between the break-up process of the elongated low-speed regions generated by the counter-rotating legs of the hairpin vortices and the break-up of dye streaks previously observed in turbulent boundary layers. Figure 17 (*a*) is a dye visualization of the lift-up and break-up of the low-speed region generated between the counter-rotating legs of the hairpin vortices. Dye is introduced into the boundary layer from a spanwise slot noted in the figure which is 10 cm ($x/\theta \approx 35$) downstream of the streamwise vortex-generation slot. Note that for this case the hairpins are not marked with dye; only the *effect* of the hairpins on the near-wall behaviour is visualized by the dye slot. Figure 17 (*b*) is a two-picture sequence of streak break-up during the bursting process as observed in a turbulent boundary layer by Runstadler, Kline & Reynolds (1963). The similarity between the two patterns illustrated by figures 17 (*a*) and (*b*) is quite obvious. Figure 17 (*c*) is a combined top–side visualization using (i) dye (introduced via the streamwise generation slot) to visualize the hairpin vortices and (ii) a sheet of hydrogen bubbles generated almost on the wall with a horizontal bubble wire to visualize the response of the near-wall fluid. This figure clearly demonstrates that the lift-up of the hydrogen bubbles is caused by the action of the counter-rotating legs of the hairpin vortex. This lift-up appears as the elongated hydrogen-bubble concentration in the top view of figure 17 (*c*), with distinctive undulations essentially identical with those viewed in figure 17 (*a*, *b*) caused by the periodic passage of the heads of the hairpins. Note also the essential similarity between the top-view hydrogen-bubble-line pattern in figure 17 (*c*) created by the hairpin vortices and the omnipresent low-speed-streak pattern observed beneath turbulent boundary layers, an example of which is shown in figure 17 (*d*).

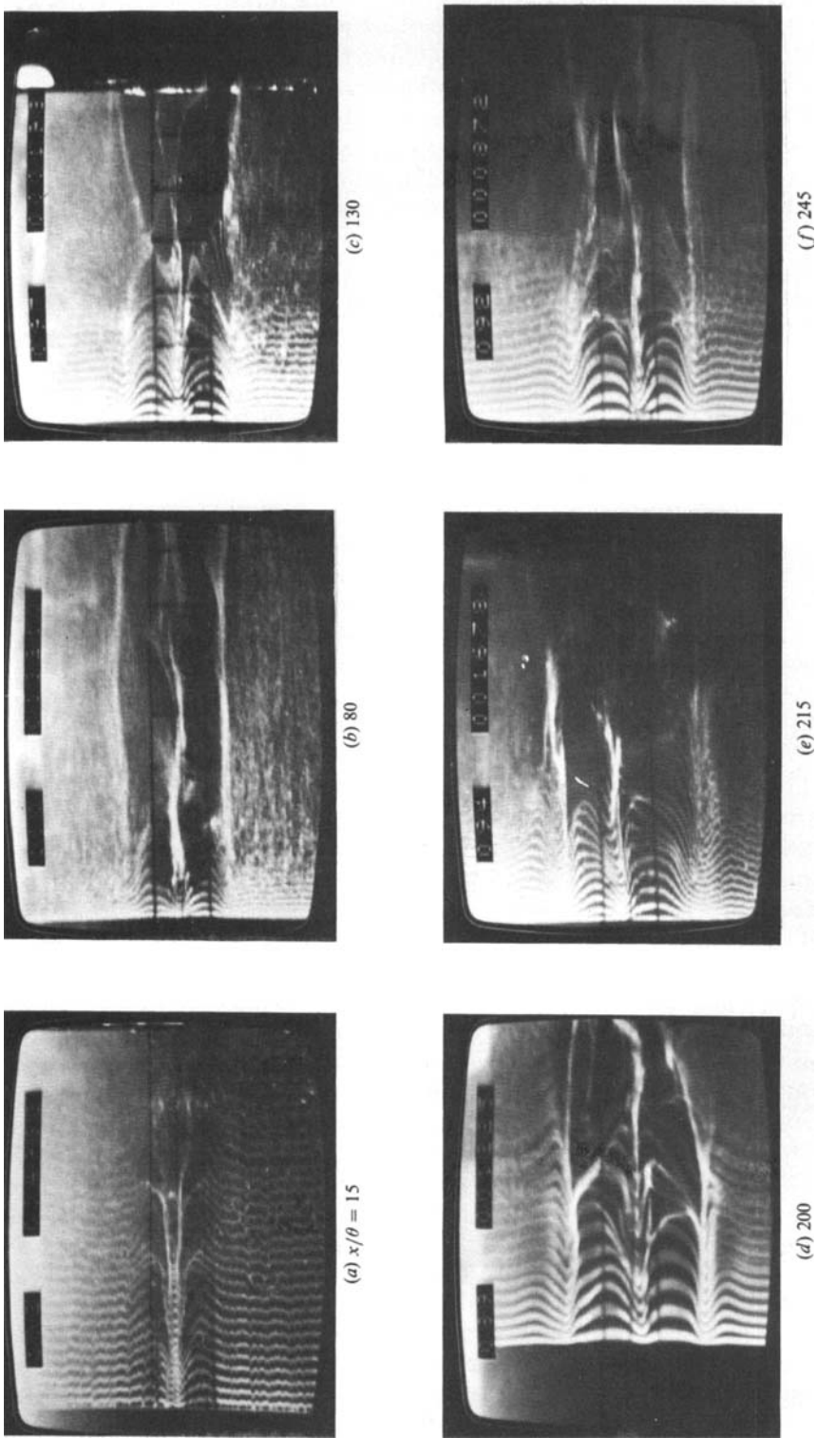

FIGURE 18. Top-view hydrogen-bubble-wire visualization of low-speed regions downstream of the synthetic streak.

The low-speed regions generated near the wall by the counter-rotating legs of the original hairpins and the secondary vortical structures were observed to extend the length of the test plate, sustaining their persistence and strength. This is illustrated in figure 18 which is developed from visualizations at a series of locations downstream of the synthetic streak. Existence of essentially the same bubble-line pattern at every downstream location demonstrates the extreme length and persistence of these low-speed regions. Interestingly, the hairpin disturbances do not demonstrate an appreciable lateral spreading, unlike the behaviour of a turbulent spot. The reason for this behaviour appears to be because the hairpin structures are generated in a *subcritical* laminar boundary layer, which remains stable to the hairpin disturbances as long as the boundary layer outboard of the structure remains subcritical (i.e. $Re_{\delta^*} \lesssim 520$).

8. Effects on velocity characteristics

8.1. *Mean-velocity behaviour*

Mean and fluctuating components of the streamwise velocity were measured at various locations downstream of the synthetic low-speed streak. The intent of this study was to determine the effect of the evolving hairpin and secondary vortices on the velocity field. Velocity profiles were measured at three lateral locations for each of five downstream stations. The three lateral locations were: (i) the plane of symmetry of the wake, corresponding to the middle of the low-speed region where low-speed fluid is lifted-up between the counter-rotating legs (this location is marked as 1 in figure 12*a*); (ii) just outboard of the plane of symmetry, marked as 2 in figure 12*a*; (iii) the region of the outer low-speed concentration, marked as 3 in figure 12(*a*).

Figure 19 is a cumulative figure of all the measured mean and r.m.s. velocity profiles measured in the wake. These profiles are plotted as a function of y/θ, where θ is the momentum thickness of the impinging laminar boundary layer at the point of hairpin formation and y is the vertical distance from the wall. Detailed velocity distributions are presented in Acarlar & Smith (1984).

Figure 19(*a*) is the mean-velocity distribution in the wake at a downstream location of $x/\theta = 13.5$, corresponding to a location 1.5 cm downstream (see figure 8) of the streamwise injection slot. Curves 1, 2 and 3 correspond to the lateral locations noted above. Note that an inflexional, high-shear layer occurs in curve 1 at approximately $y/\theta = 4$, the region of interaction between the injected low-momentum fluid and the higher-speed outer boundary-layer flow. Curve 2, obtained at the same downstream location but at a transverse location of $z/\theta = 2.25$, also demonstrates an inflexional profile. Comparing mean-velocity magnitudes, it is observed that below $y/\theta = 2.5$ the mean velocity at $z/\theta = 2.25$ is approximately 2.5 times the magnitude of that for $z/\theta = 0$, demonstrating the presence of the low-momentum injected fluid on the plane of symmetry. Since at $z/\theta = 4.5$ (curve 3) an outer low-speed concentration has not yet developed (see figure 8), the mean-velocity profile does not differ substantially from the original laminar distribution.

Figure 19(*b*) is the r.m.s of the fluctuating component of the velocity at the same downstream and lateral locations as figure 19(*a*). Curve 1 (corresponding to $z/\theta = 0$) displays two peaks, corresponding to the passage of the head ($y/\theta = 6.5$) and the counter-rotating legs ($y/\theta = 4$) of the hairpin vortices. Curve 2 ($z/\theta = 2.25$) also has two peaks, similarly corresponding to the influence of the counter-rotating legs ($y/\theta = 2.7$) and the streamwise portion of the head (at $y/\theta = 4.7$). The peak due to the streamwise portion of the head occurs at a higher y/θ value for curve 1 since the

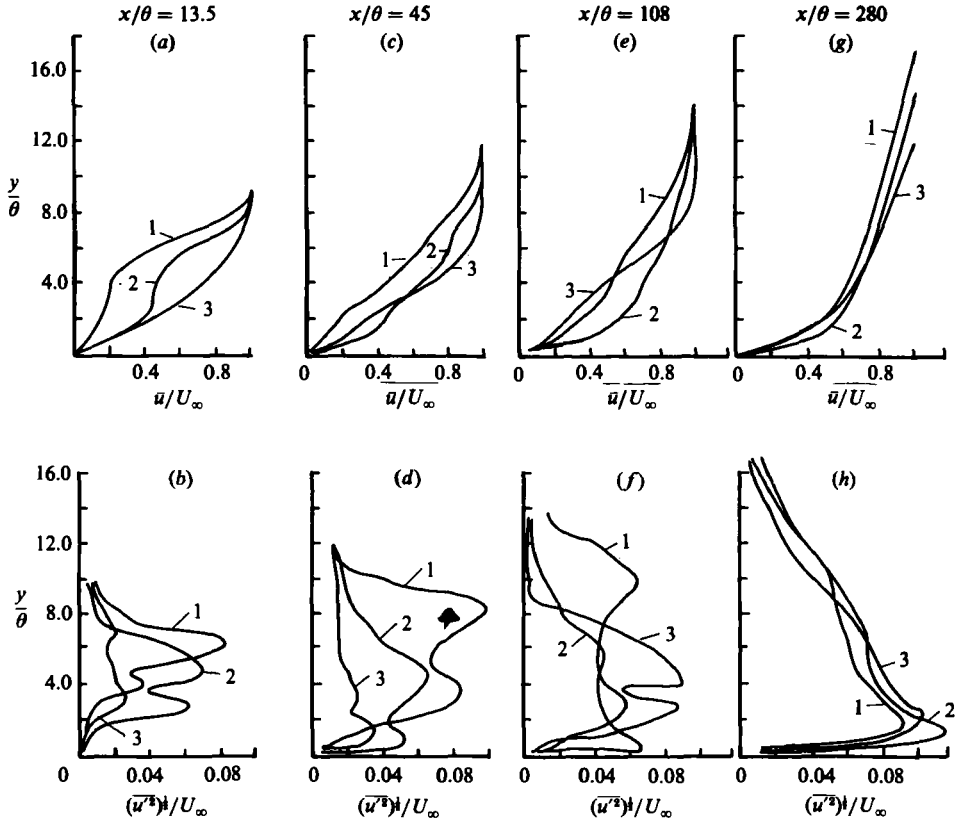

FIGURE 19. Velocity distribution in the wake at various locations downstream of a synthetic low-speed streak ($Re_\delta = 360$). Curves 1, 2 and 3 corresponds to the lateral locations shown in figure 12(*a*). $U_\infty = 12.5$ cm/s, $V_w = 1.575$ cm/s, slot size is 63.5 mm × 1 mm. Slot is located 44 cm downstream of the leading edge. $\bar{u}$, mean velocity; u', fluctuating velocity. Transverse location from the symmetry plane: curve 1, $z/\theta = 0$; curve 2, $z/\theta = 2.25$; curve 3 varies in position: (*a*), (*b*) $z/\theta = 4.5$; (*c*), (*d*) $z/\theta = 6.3$; (*e*), (*f*) $z/\theta = 7.20$; (*g*), (*h*) $z/\theta = 9.0$.

tip of the head (the transverse portion of the head) lies on the plane of symmetry ($z/\theta = 0$) and is the highest portion of the hairpin vortex. Curve 3 displays a weak peak, much lower in magnitude than demonstrated by its counterparts in curves 1 and 2, and is probably reflective of a weak influence of the developing legs of the hairpin vortex.

Figure 19(*c*, *d*) are the velocity and r.m.s. distributions at a downstream location of $x/\theta = 45$. Curve 1 of figure 19(*c*) is the mean-velocity distribution on the plane of symmetry, which indicates a marked recovery of the mean-velocity profile from its inflexional shape. Curve 2 of figure 19(*c*) is obtained at $z/\theta = 2.25$. Comparing curves 1 and 2, it is observed that for the same y/θ values the mean-velocity magnitudes are higher for curve 2. This demonstrates the persistence of the low-speed region on the plane of symmetry that was observed at $x/\theta = 13.5$ (curve 1 of figure 19*a*). Curve 3 is the mean-velocity distribution at $z/\theta = 6.30$ (transverse location 3). Lower mean-velocity magnitudes below $y/\theta = 4$, compared with curve 2, indicate the development of an auxiliary low-speed region. Visualization studies combined with the above measurements indicate that the development of the low-speed region revealed in velocity profile 3 is a result of the lift-up of low-momentum fluid from

the wall by the secondary streamwise vortical concentrations (marked as B in figure 12*b*).

Figure 19(*d*) is the r.m.s. distributions taken at the same locations as figure 19(*c*). Curve 1 (obtained at $z/\theta = 0$) again displaye two peaks, which correspond to the location of the head and the counter-rotating legs of the hairpin vortex. Comparison of curve 1 for both figure 19(*b* and *d*) demonstrates the effects of the lift-up of the head from the surface (the peak in r.m.s., due to the passage of the head occurs at a higher y/θ value in figure 19*d* compared with figure 19*b*). Comparing curves 2 in figure 19(*b* and *d*), it is observed that the lower y/θ peak (due to the passage of the counter-rotating legs) has moved closer to the wall at this location (see also figure 12). Curve 3 displays a single peak at $y/\theta = 1.5$ which reflects the development, presence and passage of the secondary, streamwise vortical concentrations on the wall.

Figure 19(*e*, *f*) are obtained at a downstream location of $x/\theta = 108$. Note that Curve 1 continues to become fuller. Curve 2 also demonstrates a similar behaviour, continuing to relax toward a fuller velocity profile. Note also that the transverse location of the outer low-speed concentrations continue to move outward with increasing downstream distance (i.e. the wake develops laterally). Thus, the z/θ location of the third lateral measurement station also increases as one moves in the downstream direction (e.g. curve 3 in figure 19*e* is located at $z/\theta = 7.20$ compared to $z/\theta = 4.5$ in figure 19*a*). Comparing curve 3 of figure 19(*c* and *e*), it is observed that the velocity profile is strongly retarded, yielding lower mean velocities at $x/\theta = 108$ than at $x/\theta = 45$. It is believed that the retardation of the velocity profile is caused by the continued lift-up of low-speed fluid by the secondary vortices which are developing outboard of the counter-rotating legs of the hairpin vortices. The bubble-line patterns illustrating the development of these types of structures are shown in figures 12(*b*) and 18.

The peaks in r.m.s. of curve 1 in figure 19(*f*) demonstrate lower magnitudes compared with figure 19(*d*), illustrating the effect of diffusion on the head of the hairpins; also note that the upper peak moves to a higher y/θ value, demonstrating the continued movement of the head away from the wall. The lower peak in curve 1 has moved much closer to the wall, compared with the lower peak at $x/\theta = 45$. The r.m.s. peaks in curve 2 also appear to relax, collapsing together and toward the wall. In contrast to figure 19(*d*), curve 3 now demonstrates two large, closely spaced peaks, essentially identical in shape with curve 2 in figure 19(*b*). The development of these two peaks is believed to be due to the head and legs of secondary vortical structures which develop at this lateral location (see Acarlar & Smith 1984). Note that these secondary vortical structures were observed in flow-visualization results to develop in this general location due to the interaction between the lifted-up low-speed regions and the higher-speed outer flow which moves toward the wall outboard of the legs of the initial hairpin vortices.

At $x/\theta = 280$, figure 19(*g*), the mean-velocity profiles at all three lateral locations have relaxed to essentially full velocity profiles, appearing quite similar. In figure 19(*h*), it can be observed that the peaks in the fluctuating component of the velocity distribution move quite close to the wall, displaying characteristics remarkably similar to those representative of a turbulent boundary layer.

From the hot-film measurements and the previously displayed visualization studies, it is apparent that passage of the hairpin vortices generates three low-speed concentration regions near the wall. These low-speed regions are extremely long and persistent, extending the entire length of the test plate. A higher-speed region (curve

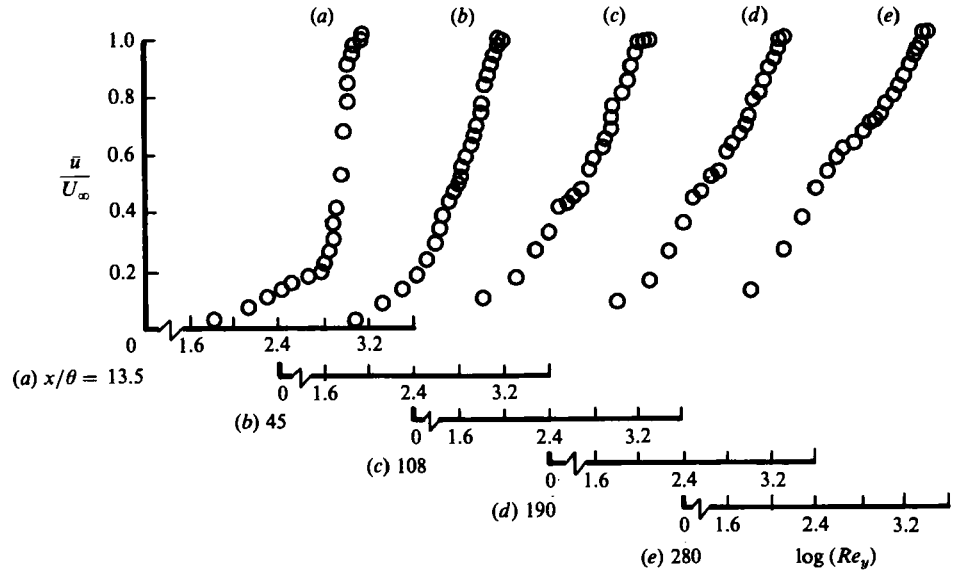

FIGURE 20. Clauser cross-plot of the mean velocity data on the plane of symmetry (curve 1) from figure 19.

2 of figure 19*a–h*) develops between these elongated low-speed regions. Visualization studies further demonstrate that the low-speed concentration on the plane of symmetry of the wake is generated by the lift-up of a low-momentum fluid by the counter-rotating legs of the hairpin vortices. The low-speed regions occurring to the sides of the hairpin legs are generated by the lift-up of low-momentum fluid by secondary streamwise vortices. These secondary vortices near the wall begin their development at about $x/\theta = 45$ (curve 3 of figure 19*d*), supporting the suggestion that these are intensified vortex-concentration regions occurring outboard of the saddle-point regions shown in figure 12(*a*).

The mean-velocity data on the plane of symmetry of figure 19 were plotted on a semi-logarithmic scale in figure 20 to determine whether the mean-velocity profile develops a logarithmic region reminiscent of a turbulent profile. Figure 20 demonstrates that at $x/\theta = 13.5$, just downstream of the synthetic streak, the outer region of the profile displays a large segment which is approximately parallel to the $\bar{u}/U_\infty$ axis. This generally straight segment appears to roughly rotate in a clockwise direction as the profile develops, finally taking the form shown at $x/\theta = 280$, which displays a strong similarity with the mean-velocity characteristic of a turbulent profile. This is a relatively remarkable result, since this logarithmic region is localized within an otherwise subcritical laminar boundary layer (figure 18 illustrates this nicely). Thus, from the observed evolution of the mean-velocity profile and the combined dye-visualization studies, it appears that the localized development of secondary vortices and the burst-like events generated by interaction of the original hairpin vortices with wall-layer fluid can give rise to a logarithmic-type mean-velocity distribution. This observation strongly supports Perry & Chong's (1982) suggestion that turbulent boundary layers are composed of a hierarchy of hairpins (older hairpins interacting with younger ones) which give rise to a mean velocity conforming to a law-of-the-wall-type velocity profile.

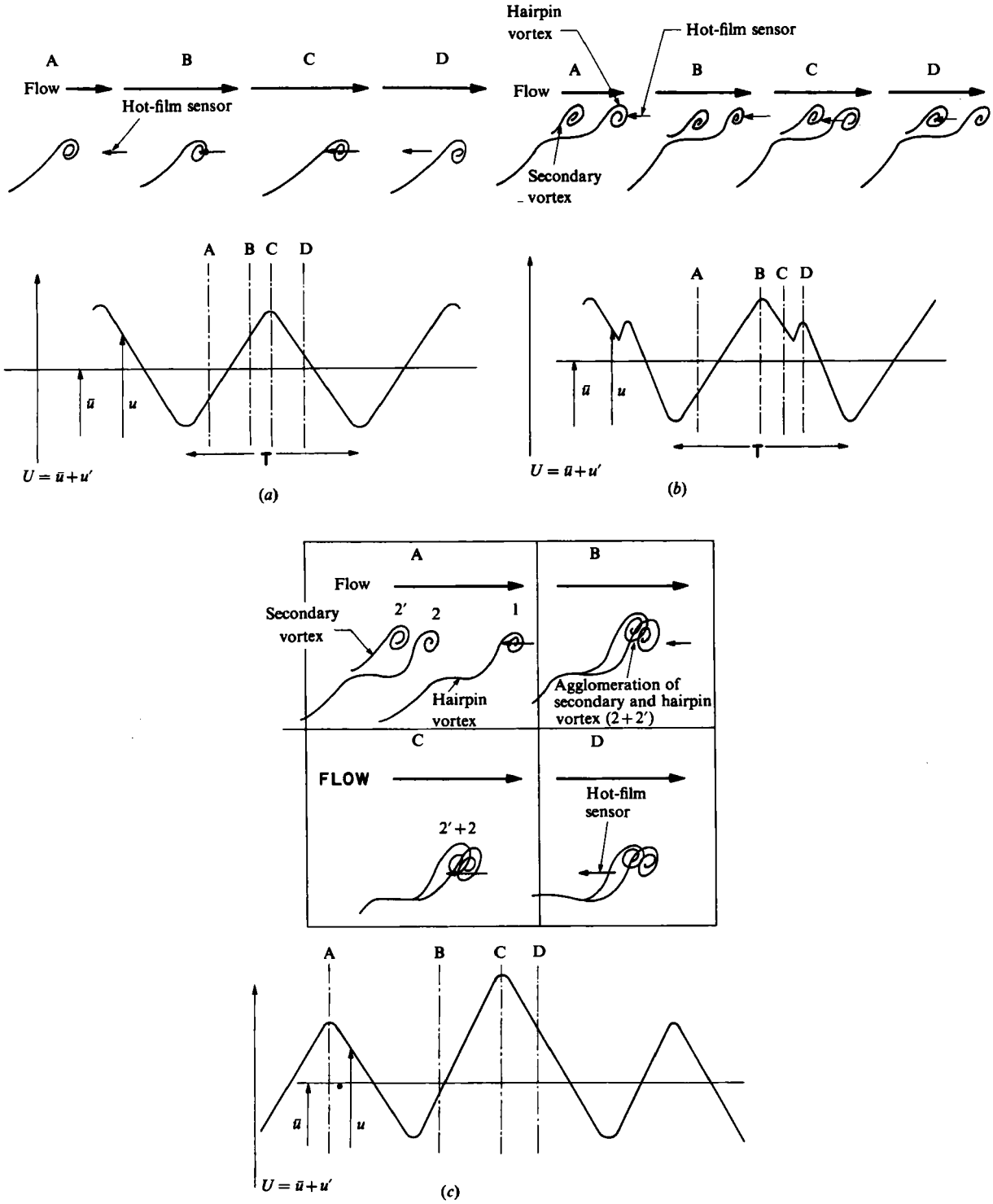

FIGURE 21. Instantaneous velocity signature $\bar{u} = u + u'$ (u is instantaneous velocity, $\bar{u}$ mean velocity, u' fluctuating velocity). (*a*) $x/\theta = 12$, $y/\theta = 6$; (*b*) $x/\theta = 90$, $y/\theta = 10$; (*c*) $x/\theta = 240$, $y/\theta = 17$.

8.2. *Instantaneous velocity behaviour*

To illustrate the time-dependent velocity behaviour caused by the generation and passage of hairpin vortices, a storage-scope display of the velocity signal from a hot-film anemometer located in the hairpin vortex street and the dye patterns of the hairpin vortices were simultaneously displayed on the video screen. The resulting velocity traces, obtained at three progressively increasing downstream locations, are shown in figure 21 in conjunction with schematics of the phase and development of the hairpin vortices.

Figure 21 (*a*) is the velocity signal at a downstream location of $x/\theta = 12$. As illustrated, the instantaneous velocity reaches a maximum just after the core of the hairpin head passes the hot-film sensor and decreases as the hairpin is carried downstream. Figure 21 (*b*) illustrates the effect of the generation of secondary vortices on the velocity signal. Following the passage of the head of a hairpin vortex, secondary vortices, which develop between the interface of the lifted-up low-momentum wall-region fluid and higher-speed outer boundary-layer flow, are detected by the hot-film sensor as a lower-amplitude, secondary harmonic. At a downstream location of $x/\theta = 240$, agglomeration and interaction of the secondary and initial hairpin vortices result in the burst-like events described in § 6 and illustrated in figures 14–16. As shown in figure 21 (*c*), the effect of this rapid ejection behaviour is detected in the velocity signal as a higher than normal peak.

9. Geometric and rotational characteristics

Several parameters characterizing the hairpin vortices spawned by the synthetic low-speed streak were evaluated from the flow-visualization results. The evaluated parameters are: geometric size and shape of the hairpin vortex at various locations downstream of the synthetic streak; typical core diameters D_c; circulation Γ; and convection velocity of the head of the hairpin vortices. There are a variety of experimental methods available to evaluate the above parameters for two-dimensional vortices and vortex rings such as flow visualization, hot-film anemometry, and laser-Doppler velocimetry (LDV). However, owing to structure-to-structure variations in the characteristics of individual hairpins, the three-dimensionality of the flow, non-uniform stretching, and the continuous evolution of the hairpin vortices, it is impractical, if not impossible, to determine circulation using LDV or hot-film-anemometry techniques. In this study, dye and hydrogen-bubble visualization are used to determine the above parameters.

9.1. *Geometric characteristics*

Once a hairpin vortex is generated, it deforms non-uniformly since three-dimensionalities and mutual induction effects cause different portions of the vortex to migrate at different rates through the surrounding boundary layer with its varying velocity gradient. Thus, the shape and the size of a hairpin vortex will undergo a continuous evolutionary process. In the present study, the geometric variations in the hairpin vortex at various downstream locations were determined using both hydrogen-bubble and dye visualization. The evolving hairpin shapes presented in figure 22 were obtained from a side-view dye-visualization sequence taken from a reference frame translating with the vortex (i.e. the dye patterns are for the *same* hairpin vortex obtained at a series of downstream locations), as described in §2. Dye

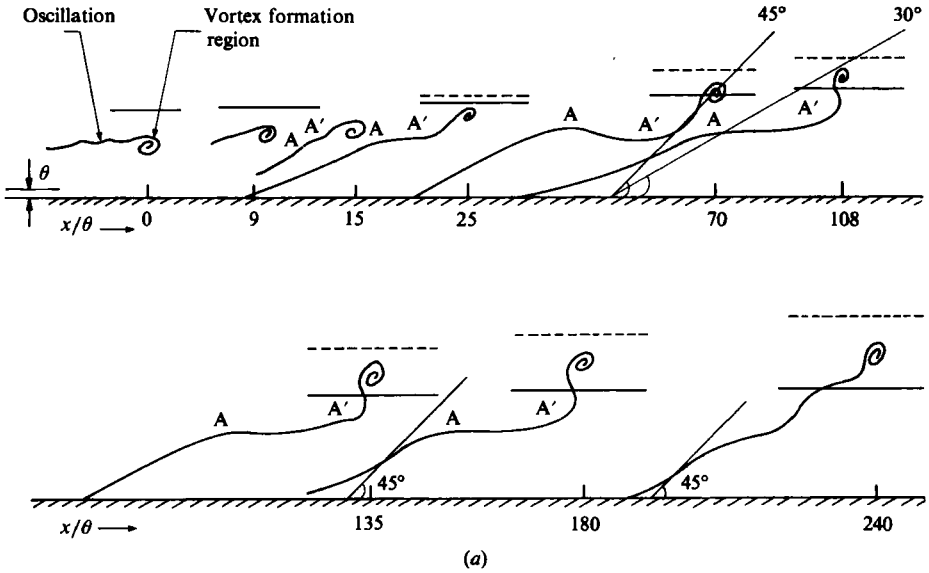

(*a*)

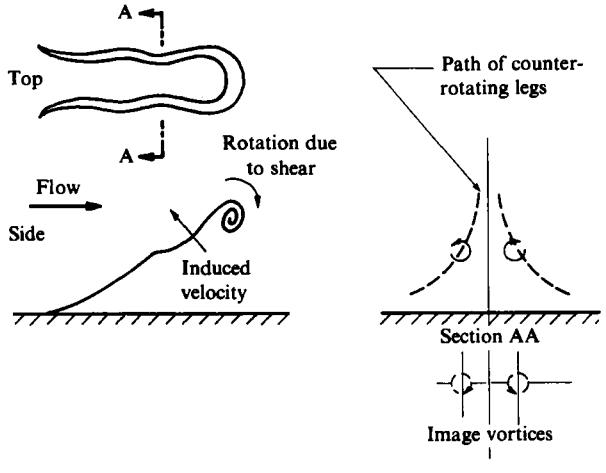

(*b*)

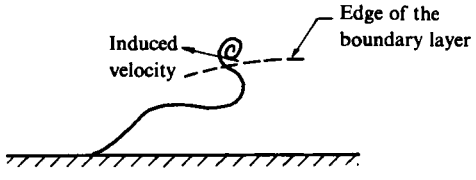

(*c*)

FIGURE 22. (*a*) Evolution and dimensions of a hairpin vortex downstream of the synthetic streak. $Re_\theta = 150$, $Re_{V_w} = 17$, $V_w/U_\infty = 0.150$. ——, laminar boundary-layer thickness; – – –, boundary-layer thickness due to presence of hairpins. (*b*) Schematic of the portion of the legs migrating together as they lift-up from the surface. (*c*) Curling back of the head when it is out of the boundary shear layer.

patterns were traced onto clear plastic sheets from a series of hard-copy prints from a video-graphic printer (see Smith 1982).

Figure 22(*a*) illustrates the evolution of the hairpin vortex as it proceeds downstream. At the point of formation, the angle that the legs make with the wall is less than 10°. Mutual induction effects cause the forward portion of these legs and the head of the vortex to move away from the wall as shown in figure 22(*a*) (this begins about $x/\theta \approx 10$). Since the trailing portion of the legs must connect back to lateral vorticity sheets near the wall, that trailing portions of the legs undergo extreme stretching by the local velocity gradient. This stretching further increases both the induced velocities and the concentration of vorticity in the core of the legs.

A portion of these legs, which move into outer regions owing to mutual induction effects, migrate together owing to image-vortex effects as shown in figure 22(*b*). Since the legs are of opposite vorticity, as they approach each other they begin to interact through viscous effects such that mutual vorticity cancellation begins to take place (a process suggested by Head & Bandyopadhyay 1981).

Head & Bandyopadhyay (1981) suggest that a hairpin vortex in a shear layer will be under the influence of two opposing effects. The first of these is a shear effect which tends to rotate the hairpin back towards the wall. This effect is opposed by the induced velocity that each leg of the hairpin imposes upon the other. They suggest that the angle at which the hairpin reaches equilibrium will be the result of the interaction between these two opposing effects. It is believed that the reduction of the vorticity in the portions of the legs of the hairpin that closely approach each other will reduce the induced velocity of those parts of the legs, creating an imbalance towards the shear effect. A portion of the weakened legs will subsequently be pushed towards the wall by the shear flow, initiating a kinked region (labelled AA′) which is observed beginning at approximately $x/\theta \approx 15$ in figure 22(*a*). As the mutual vorticity-cancellation effects proceed, the weakened portions of the legs (AA′) will rotate further towards the wall under the influence of the shear effect. Note that once the head of the hairpin vortex is out of the boundary layer, it will only experience the effect of induced velocities. This effect causes the tip of the hairpin to curl back upstream as illustrated in figure 22(*c*). For a more detailed discussion of the hairpin deformation dynamics the reader is referred to Part 1 of this study (Acarlar & Smith 1987).

Figure 23 is the variation in the convection velocity of the tip of a hairpin vortex with downstream location (obtained for the vortex shown in figure 22). Since the hairpin vortex is generated inside the boundary layer, its initial velocity after the roll-up process is observed to be $0.52U_\infty$, with this velocity increasing rapidly as the head rises through the boundary layer. Although the head curls back when it is outside the boundary layer, its convection velocity still remains lower than the free-stream velocity (at approximately $x/\theta = 108$ the head has curled back, but its convection velocity is $0.86U_\infty$). The defect in the convection speed is believed to be due to the induced velocity of the curled-back portion of the head, which is in opposition to the free-stream velocity (see figure 22*c*). Smith (1978) observed that a coherent flow structure, which could be associated with the lift-up and burst-type behaviour in a turbulent boundary layer, would initially be observed to convect at velocities on the order of $0.4U_\infty$, accelerating as they moved up and away from the surface, similar to the behaviour illustrated here. In addition, Smith observed that outer-region disturbances with convection velocities of 0.60–$0.70U_\infty$ seemed to be those most associated with the lift-up of wall-region fluid. Examining figure 23 it is observed that the hairpins attain this velocity range at a downstream location of

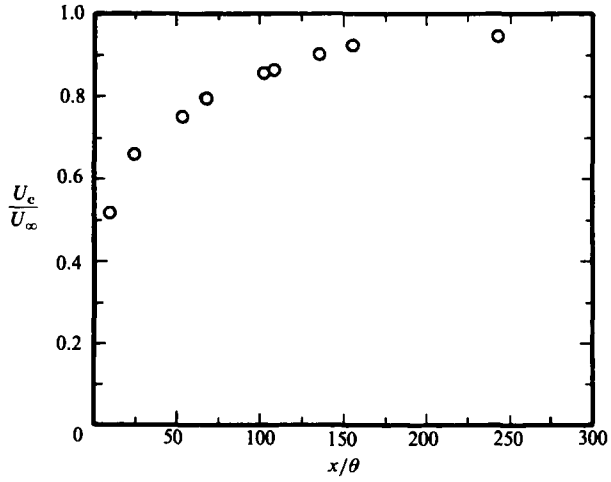

FIGURE 23. Relative streamwise velocity, U_c/U_∞, of the head of a hairpin vortex at various downstream locations.

$x/\theta \approx 15$–25, where the present study shows that lift-up of fluid by the counter-rotating legs of the hairpin vortex is first noted. The similarity of these observations suggests that what Smith observed as transverse vortical structures were actually the heads of convecting hairpin vortices (which he speculates they may be).

Core sizes of the transverse head and the streamwise legs of the hairpin vortices were determined for selected cases using combined top–side- and top–end-view hydrogen-bubble-wire visualization techniques respectively. A typical end-view picture obtained using a horizontal hydrogen-bubble wire and the end-view-mirror visualization technique (described in §2) is shown in figure 12(*a*). In this figure bubble lines that originate from a height of $y/\theta = 4.3$ lift-up and concentrate in the core of the hairpin vortex, thus assisting in the measurement of the core sizes. From this figure, the ratio of the core diameter D_c, to momentum thickness θ (momentum thickness of the impinging laminar boundary layer at the point of formation), is measured as $D_c/\theta \approx 1.7$. Figure 24 is a typical top–side hydrogen-bubble visualization used to determine the dimensions of the transverse head of a hairpin vortex. For the case shown in figure 24, D_{ch}/θ is measured as 2.4. It should be noted that the visible (apparent) diameter may not necessarily be the actual diameter of the vortex core. It was shown by Schwartz (1981) that unless a bubble line is generated in the centre of a vortex core, there is no accurate way to measure the actual vortex-core size. However, assuming that the motion is irrotational outside the core (as for a Rankine combined vortex), these apparent diameters can be used in estimating vortex circulation strength, as will be described in the following section.

9.2. *Rotational characteristics*

For selected cases, the vorticity of the head ω_x, the streamwise legs ω_x, and of the standing vortex ω_z were determined visually from the bubble-line patterns. It is assumed that various cross-sections of the hairpin and the standing vortex can be approximated as combined Rankine-type vortices. Outside the core, accurate determination of vorticity from the bubble-line patterns is not possible. Within the vortex core, it was assumed that $V_\theta = \Omega r$, where Ω represents the solid-body rotational speed. Vorticity was determined from bubble lines marking the core of the

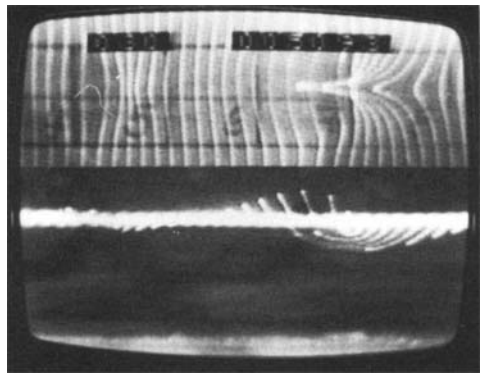

FIGURE 24. Transverse head of a hairpin vortex. $Re_\theta = 135$, $x/\theta = 48$, $Re_{V_w} = 17$, $V_w/U_\infty = 0.150$.

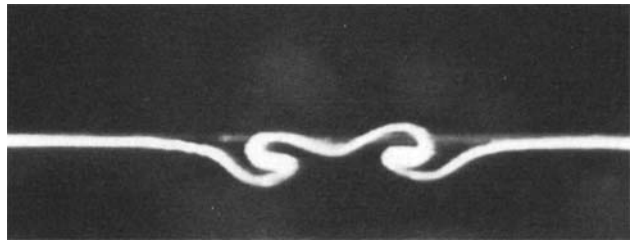

FIGURE 25. End-view hydrogen bubble visualization used to determine the circulation of counter-rotating legs. $Re_\theta = 135$, $x/\theta = 48$, $Re_{V_w} = 17$, $V_w/U_\infty = 0.150$.

vortex by measuring the angle of rotation of a bubble-line and the corresponding period over which that rotation takes place. The average angular velocity Ω is determined by dividing the angle rotated by the time interval. The vorticity is approximated as twice this angular velocity.

Once ω is determined, it is non-dimensionalized on the velocity gradient at the wall:

$$\omega^+ = \left.\frac{2\Omega}{\partial u/\partial y}\right|_{\text{wall}} = \left.\frac{\omega}{\partial u/\partial y}\right|_{\text{wall}}.$$

Outside the core of a vortex, if the motion is assumed to be irrotational (as for a combined Rankine-type vortex), a line integral about the core will yield a value for circulation reflecting the strength of the core alone. Thus

$$\Gamma = V_\theta \pi 2 r_c, \quad V_\theta = \Omega r_c$$

where r_c is the radius at a point of measurement and Ω the rotational velocity at r_c. Thus

$$\Gamma = \Omega 2\pi r_c^2 = \tfrac{1}{2}\pi D_c^2 \Omega,$$

with non-dimensional circulation given by

$$\Gamma^+ = \frac{\Gamma}{\nu}.$$

Using the above equations and procedure, the vorticity and circulation of the transverse head and counter-rotating legs were determined for selected cases. All the

magnitudes given below are mean values obtained from thirty measurements carried out for each case.

Figure 25 is an end-view hydrogen-bubble-visualization picture obtained from a sequence used to determine the circulation of the counter-rotating legs. For the sequence, the average values for the non-dimensional vorticity, ω_z^+ and circulation Γ_z^+ were determined as 0.938 and 99 respectively for a case with $V_w/U_\infty = 0.150$, $Re_{\delta^*} = 350$ and $x/\theta = 48$. For the same downstream location and Reynolds number, the average values of the non-dimensional vorticity and the circulation for the transverse head were determined to be 1.48 and 528. Thus, the circulation strength of the counter-rotating legs appears to be approximately one-fifth that of the head. Note that this ratio is similar to a one-seventh ratio determined for hairpin vortices generated by hemisphere shedding and reported elsewhere (Acarlar & Smith 1987). An uncertainty analysis indicates that the uncertainties for the measured vortices and circulations are large (up to $\pm 40\,\%$). However, this implies that the circulation of the transverse head is at worst three times the circulation of the counter-rotating legs. The low value of circulation for the counter-rotating legs is believed to be due to (i) the mutual vorticity-cancellation effects that they impose upon each other and (ii) vorticity transfer to wall-layer fluid through viscous effects (see Ersoy & Walker 1985). Note that for the transverse head there is no similar mechanism by which the transverse circulation of the hairpin tip can be reduced, except when it is in close proximity to the bounding surface.

10. Effect of outer-region flow structures on synthetic-streak breakdown

A number of previous studies have suggested that inner–outer layer interaction plays an important role in the production of turbulence in turbulent boundary layers (Offen & Kline 1974, 1975; Townsend 1956; Hinze 1975; Kline 1978; Wallace 1982; Smith 1984). In particular, Offen & Kline (1974, 1975) suggest that the burst event observed in turbulent boundary layers is the result of an interaction between a transverse head of a previous burst and a low-speed streak. Furthermore Wallace (1982) and Smith (1984) have suggested that local pressure-field fluctuations distort and destabilize shear layers diffusing from the wall, causing hairpin vortices to form. To examine the proposed influence of outer-region disturbances on wall-region behaviour, the following study was performed with the synthetic-streak test section.

Outer-region boundary-layer fluctuations and previous burst structures were experimentally simulated using hairpin vortices shedding at a constant frequency from a hemisphere (for a discussion of the shedding behaviour see Acarlar & Smith 1987). A hemisphere of 0.762 cm was placed in an initially laminar boundary layer 4.6 cm upstream of the synthetic-streak generating slot. The effect of the passage of the hairpin vortices on the behaviour of the synthetic streak was then examined for various slot injection rates.

Figure 26(*a*) is a side-view visualization of a stable low-speed, synthetic streak marked with dye in the injection fluid. The Reynolds number based on the momentum thickness of the impinging laminar boundary layer is $Re_\theta = 114$, $V_w/u_\infty = 0.144$. Figure 10 indicates that for these conditions the synthetic streak is stable and no hairpin vortices are generated; hot-film measurements confirmed the streak stability. Figure 26(*b*) shows the effect of the hemisphere-shed hairpin vortices on the same low-speed synthetic streak of figure 26(*a*). To obtain this picture, a vertical hydrogen-bubble wire is located just upstream of the streamwise slot and the height of the bubble wire above the flat plate is adjusted to mark only the heads of

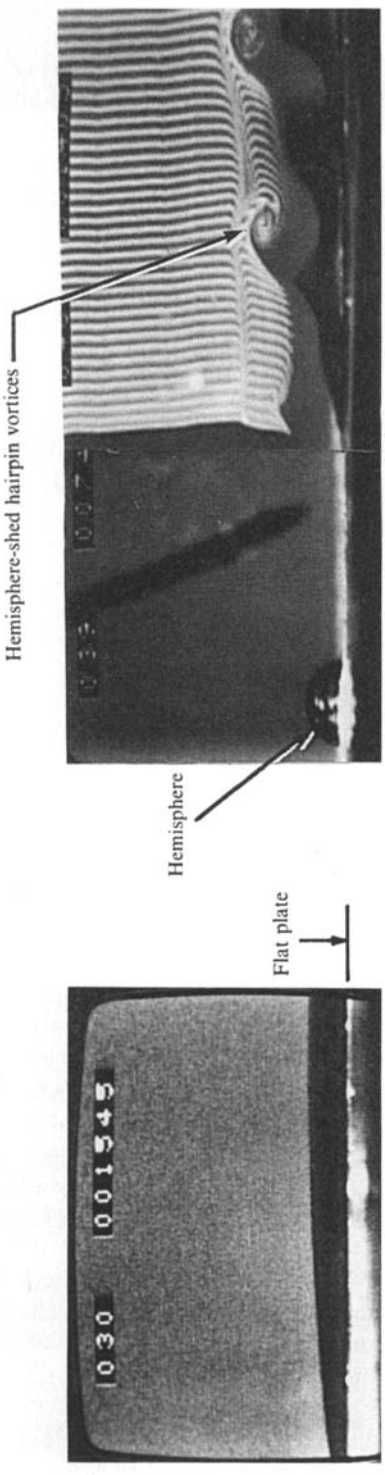

FIGURE 26. Effect of hemisphere-shed hairpin vortices on the stable synthetic streak. (*a*) Side view of a stable low-speed synthetic streak, $Re_\theta = 114$, $Re_{V_w} = 11.3$, $V_w/V_\infty = 0.144$. (*b*) Hemisphere-shed hairpin vortices causing the break-up of the stable synthetic streak. The injection and free-stream velocity are as for (*a*).

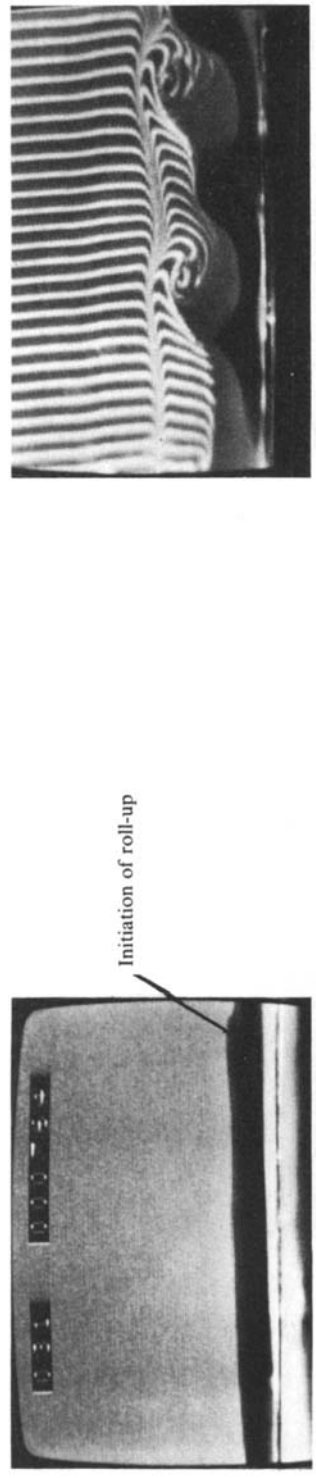

FIGURE 27. Effect of hemisphere-shed hairpin vortices on already shedding synthetic low-speed streak. (*a*) Side view of a critical synthetic streak. $Re_\theta = 114$, $Re_{V_w} = 14.1$, $V_w/U_\infty = 0.180$. (*b*) Hemisphere-shed hairpin vortices on synthetic streak.

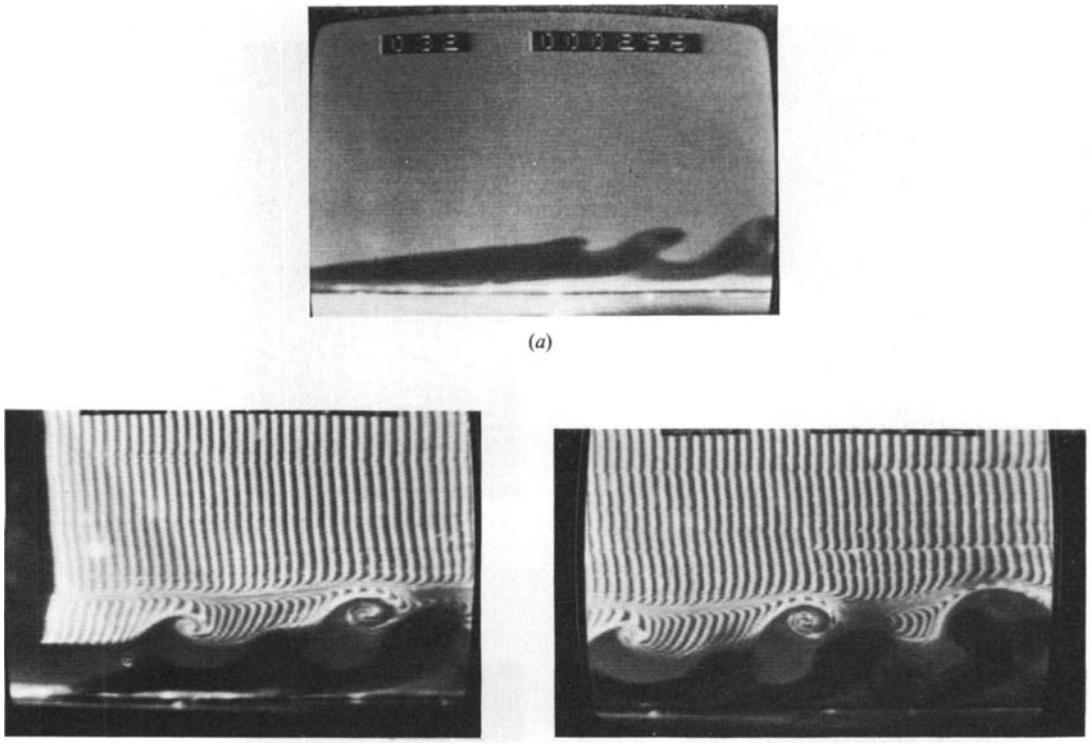

(*a*)

(*b*) (*c*)

FIGURE 28. Effect of hemisphere-shed hairpin vortices on already shedding synthetic low-speed streak. (*a*) Roll-up of synthetic streak in the absence of upstream hemisphere. $Re_\theta = 114$, $Re_{Vw} = 17$, $V_w/U_\infty = 0.217$. (*b*) Modification of roll-up characteristics of the synthetic streak of figure (*a*) due to the presence of hemisphere-shed vortices. $x/R = 6$. (*c*) Interaction and agglomeration of hemisphere-shed and synthetic-streak break-up hairpin vortices. $x/R = 10$.

the hairpins generated by the hemisphere. As the hairpins pass over the synthetic low-speed streak, they cause it to break-up into vortical structures. The break-up occurs at the passage frequency of the hemisphere hairpins. For the case shown in figure 26(*b*), the shedding frequency of the hemisphere was 1.66 Hz. From a comparison of figure 26(*a*, *b*) it is clear that the hemisphere vortices, moving in the outer portion of the boundary layer, interact strongly with the synthetic-streak region, causing the streak to destabilize and roll-up into vortical structures with the same frequency as the disturbance. A similar type of eruption of a laminar boundary layer is demonstrated by Doligalski, Smith & Walker (1980) and Doligalski & Walker (1984) to occur because of the passage of a two-dimensional, convecting vortex above a plane wall.

Increasing the injection rate to $V_w/U_\infty = 0.180$ caused the low-speed streak to become increasingly unstable. Figure 27(*a*) shows this case, which just reveals the initiation of a roll-up. Note that the formation of hairpin vortices occurs in an irregular manner for this marginally critical flow condition. Figure 27(*b*) shows the response of the same synthetic streak to the hemisphere-shed vortices. The low-momentum fluid of the synthetic streak (marked with dye) is lifted up by the head and counter-rotating legs of the hemisphere-shed vortices (marked by the bubble

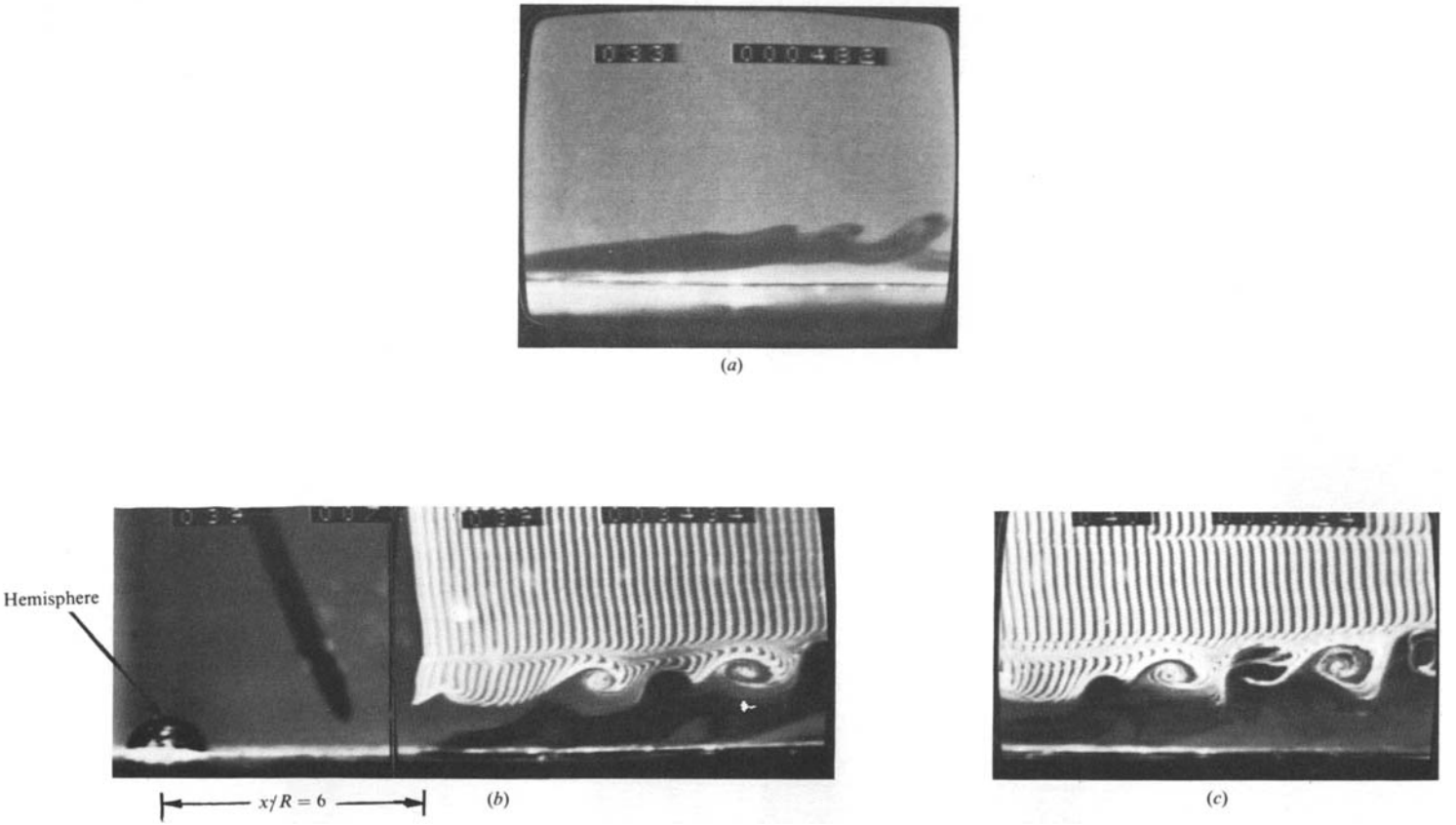

FIGURE 29. Effect of hemisphere-shed hairpin vortices on already shedding synthetic low-speed streak. (*a*) Roll-up of synthetic streak in the absence of upstream hemisphere. $Re_\theta = 114$, $Re_{V_w} = 22.6$, $V_w/U_\infty = 0.288$. (*b*) Modification of roll-up characteristics of the synthetic streak of (*a*) due to the presence of hemisphere-shed vortices: $x/R = 6$. (*c*) Interaction and agglomeration of hemisphere-shed and synthetic-streak break-up hairpin vortices: $x/R = 10$.

lines), precipitating the break-up of the synthetic-streak fluid into hairpin-type vortices, again at a frequency equivalent to the hemisphere shedding frequency.

Further increasing the injection rate (in the absence of the hemisphere) resulted in the initiation of an oscillation which breaks down into a periodic series of hairpin-type vortices as shown in figure 28(*a*). The frequency of vortex roll-up for the flow conditions shown in figure 28(*a*) is 2.04 Hz. Placing the hemisphere upstream of the already shedding synthetic streak results in a modification of the roll-up characteristics as shown in figure 28(*b*); the roll-up frequency for the synthetic streak is phase-locked to the hemisphere shedding frequency, decreasing to 1.66 Hz. Note that the lift-ups that roll-up into hairpin vortices (marked with dye) occur between the hemisphere-generated vortices (marked with bubble lines). Figure 28(*c*), obtained at a location further downstream ($x/\theta = 40$), shows that the hemisphere-shed hairpin vortices and the hairpins generated from the synthetic streak agglomerate and interact in a three-dimensional pairing process. This pairing process appears to behave somewhat chaotically, with the resulting structures moving suddenly away from the surface in a manner similar to both (i) the interaction process described in § 6, and (ii) the break-up stage of the Kline *et al.* (1967) turbulent burst event as observed in turbulent boundary layers.

For an injection rate of $V_w/U_\infty = 0.288$, figure 29(*a*), the natural roll-up frequency of the undisturbed synthetic streak was observed to be 2.8 Hz. Placing the hemisphere upstream of the synthetic streak again modifies the streak behaviour, imposing the hemisphere shedding frequency of 1.66 Hz on the streak break-up. Note that at this injection rate the transverse heads of the hairpin vortices generated by the modified break-up of the synthetic streak (marked with dye) lift-up much faster compared with figure 28(*b*) and interact more strongly with the hemisphere-shed vortices. The result is again a three-dimensional pairing process that suddenly lifts-up away from the surface.

Further studies were carried out up to an injection rate of $V_w/U_\infty = 0.432$, and it was observed that for all the injection rates the roll-up frequency of the synthetic streak remained constant at the hemisphere shedding frequency of 1.66 Hz.

The above results strongly support the earlier suggestions that the outer flow interacts with the near-wall low-speed streaks, modifying and manipulating their behaviour. It can also be speculated that if the strength of the outer disturbance is sufficiently strong, the roll-up frequency of the low-speed streak will synchronize with the passage frequency of the disturbance.

11. Summary and discussion

The results of the above studies have shown that under the proper conditions streamwise low-momentum-fluid regions introduced beneath an initially subcritical laminar boundary layer will become unstable and break down to form hairpin-type vortices. The periodicity and repeatable characteristics of this process have enabled the study of both the individual evolution and three-dimensional interaction of these hairpin vortices. In previous studies of turbulent boundary layers, it is suggested that the origin and generation of hairpin vortices in a turbulent boundary layer are due to the distortion and destabilization of the low-speed regions diffusing from the wall (Kim *et al.* 1971; Wallace 1982; Smith 1984). The development of hairpin vortices due to the flow over and around a local streamwise low-speed region strongly supports the above suggestions regarding the origin of hairpin vortices in turbulent boundary layers.

It was observed that once a horseshoe vortex is generated, it is stretched by the wall-shear layer. Biot–Savart interactions between the various portions of the vortex amplify the distortion of the vortex leading to the development of a hairpin shape which displays a self-induced movement away from the wall. Portions of the counter-rotating legs that move away from the wall migrate together owing to image-vortex effects; viscous interaction between the portions of the legs result in a mechanism of mutual vorticity cancellation, which gives rise to an apparent 'kinking' in the geometry of the hairpin, as shown in figures 5 and 22.

Since the trailing portions of the hairpin legs connect back to the lateral vorticity sheets diffusing from the wall, the trailing portions of the legs undergo extreme stretching by the local velocity gradient, and remain in close proximity to the surface. These portions of the trailing legs that remain near the surface develop strongly amplified vorticity concentrations as a result of stretching and three-dimensional agglomeration of the streamwise legs of sequential hairpin vortices. The lateral pressure gradients created by these counter-rotating legs cause the accumulation and concentration of low-momentum fluid between the legs by the vortex interaction mechanism suggested by Doligalski & Walker (1984). This effect provides the mechanism to both pump low-momentum fluid away from the surface and develop an extremely long and persistent low-speed concentration downstream of the synthetic streak.

A high-shear layer is generated at the interface between the lifted-up low-momentum fluid and the higher-speed outer boundary-layer flow. This shear layer rolls-up into secondary vortices by essentially the same mechanism suggested by Doligalski *et al.* (1980). These secondary vortices strongly interact with the original hairpins, generating chaotic structures which suddenly eject away from the wall. These events appear very similar to the break-up stage of the burst sequence observed in turbulent boundary layers.

In addition to the low-speed concentration generated between the counter-rotating legs, two other elongated low-speed regions are created to either side of the plane of symmetry of the wake. It is observed that these lateral low-speed regions are created due to a lift-up of low-momentum fluid by secondary streamwise vortices near the wall. These secondary vortical structures (marked as B in figure 12*a*) are believed to be generated owing to the distortion and intensification of vorticity by the inrush of fluid outboard of the counter-rotating legs of the hairpin vortices. Details of the generation mechanism of these secondary vortices is schematically illustrated in figure 12(*a*).

Hot-film measurements indicate that a strong inflexional velocity profile is present just downstream of the synthetic streak. The velocity profiles evolve with downstream distance, yielding fuller profiles which eventually begin to resemble that of a turbulent boundary layer. Combined visualization and hot-film measurements show that transition of the velocity profiles to a turbulent-type profile requires the interaction of the secondary vortices with the hairpins, creating sudden ejections away from the wall. This result supports the earlier arguments of Perry & Chong (1982) which suggest that a hierarchy of hairpin vortices must exist in order for the mean-velocity profile to behave logarithmically.

Dye and hydrogen-bubble visualization of the near-wall, low-speed regions (generated by the presence of the hairpin vortices) illustrate that these low-speed regions first lift-up, oscillate violently in a three-dimensional manner, and then break-up into smaller-scale motions following the passage of a hairpin over them. It was observed that the lift-up is caused essentially by the counter-rotating legs of the hairpin vortex

(see figure 17*c*). This lifted-up low-momentum fluid is caught up by various sections of the hairpin, giving the appearance of an oscillation which is then carried away from the wall and downstream. This process occurs in a manner very similar to the streak break-up process described during the bursting in turbulent boundary layers, as visualized and described by Kline *et al.* (1967), and Bogard (1982).

Simulation of outer-region disturbances of a turbulent boundary layer using hemisphere-shed vortices demonstrates the strong interaction that can occur between inner and outer regions of a boundary layer. The results indicate that an inner-region synthetic streak will phase-lock with the passage of outer-region disturbances, becoming unstable and rolling-up at the passage frequency of the outer-region disturbance.

The results presented above have clarified many of the characteristics of generation and interaction of both hairpin vortices and low-momentum streak-type regions near a surface. It has been observed that hairpin vortices can originate from the roll-up of three-dimensional shear layers. These hairpins can generate extremely long and persistent low-speed concentrations between their counter-rotating legs, demonstrating their potential role in the formation of the low-speed streaks of turbulent boundary layers. Secondary vortices generated by the interaction between the lifted-up low-speed fluid and the higher-speed outer boundary-layer flow were observed to interact strongly with the original hairpin vortices, creating 'burst-like' events similar to the mechanism required for the turbulent bursting process. On the basis of the above results, it appears that a strong case can be made for the presence, if not dominance, of hairpin vortices in the wall region of turbulent boundary layers.

The authors wish to thank Dr J. David A. Walker and Mr A. Haji-Haidari for their advice and assistance. We also wish to thank the Air Force Office of Scientific Research for its support of this research. The continuing support of the AFOSR is gratefully acknowledged.

REFERENCES

ACARLAR, M. S. & SMITH, C. R. 1984 An experimental study of hairpin-type vortices as a potential flow structure of turbulent boundary layers. *Rep.* FM-5, Department of Mechanical Engineering and Mechanics, Lehigh University.

ACARLAR, M. S. & SMITH, C. R. 1987 A study of hairpin vortices in a laminar boundary layer. Part 1. Hairpin vortices generated by a hemisphere protuberance. *J. Fluid Mech.*, **175**, 1–41.

ACHIA, B. U. & THOMPSON, D. W. 1976 Structure of the turbulent boundary in drag-reducing pipe flow. *J. Fluid Mech.* **81**, 439–464.

BACHER, E. V. & SMITH, C. R. 1985 An experimental study of the modifying effects of a streamwise grooved surface of triangular cross-section on the flow structure and statistical characteristics of turbulent boundary layers. *Rep.* FM-8, Department of Mechanical Engineering and Mechanics, Lehigh University.

BLACKWELDER, R. F. & ECKELMANN, H. 1979 Streamwise vortices associated with the bursting phenomenon. *J. Fluid Mech.*, **94**, 577–94.

BLACKWELDER, R. F. & KAPLAN, R. E. 1971 Intermittent structures in turbulent boundary layers. *AGARD Conf. Proc.* **43**, 5.1–5.7.

BOGARD, D. G. 1982 Investigation of burst structures in turbulent channel flows through simultaneous flow visualization and velocity measurements. Ph.D. Dissertation, Department of Mechanical Engineering, Purdue University.

BRODKEY, R. S. & WALLACE, J. M. 1982 The Delta Conferences. *NSF Project Report*. The Ohio State Research Foundation, Columbus, Ohio.

DOLIGALSKI, T. L., SMITH, C. R. & WALKER, J. D. A. 1980 A production mechanism for turbulent boundary layers. In *Viscous Drag Reduction* (ed. G. Hough); *Prog. Astro. Aero.*, **72**, 47–72.

DOLIGALSKI, T. L. & WALKER, J. D. A. 1984 The boundary layer induced by a convected two-dimensional vortex. *J. Fluid Mech.* **139**, 1–28.

ERSOY, S. & WALKER, J. D. A. 1985 Viscous flow induced by counter-rotating vortices. *Phys. Fluids* **28**, 2687–2698.

HEAD, M. R. & BANYOPHADYAY, P. 1981 New aspects of turbulent boundary-layer structure. *J. Fluid Mech.* **107**, 297–337.

HINZE, J. O. 1975 *Turbulence*, 2nd edn. McGraw-Hill.

KIM, H. T., KLINE, S. J. & REYNOLDS, W. C. 1971 The production of turbulence near a smooth wall in a turbulent boundary layer. *J. Fluid Mech.* **50**, 133–160.

KLINE, S. J. 1978 The role of visualization in the study of the structure of the turbulent boundary layer. *Lehigh Workshop on Coherent Structure in Turbulent Boundary Layers* (ed. C. R. Smith & D. E. Abbott), pp. 1–27.

KLINE, S. J., REYNOLDS, W. C., SCHRAUB, F. A. & RUNSTADLER, P. W. 1967 The structure of turbulent boundary layers. *J. Fluid Mech.* **30**, 741–773.

LAUFER, J. & NARAYANAN, M. A. 1971 Mean period of the turbulent production mechanism in a boundary layer. *Phys. Fluids* **14**, 182.

LEE, M. K., ECKELMANN, L. D. & HANRATTY, T. J. 1974 Identification of turbulent wall eddies through the phase relation of the components of the fluctuating velocity gradient. *J. Fluid Mech.* **66**, 17–34.

LU, L. J. & SMITH, C. R. 1985 Image processing of hydrogen bubble flow visualization for determination of turbulence statistics and bursting characteristics. *Exps Fluids*, **3**, 349–356.

MOIN, P. & KIM, J. 1985 The structure of the vorticity field in turbulent channel flow. Part 1. Analysis of instantaneous fields and statistical correlations. *J. Fluid Mech.* **155**, 441–464.

MORROW, T. B. & KLINE, S. J. 1974 The performance of hot-wire and hot-film anemometers used in water. *Flow: Its Measurement and Control*, no. 1, Instr. Soc. Amer.

NAKAGAWA, H. & NEZU, I. 1981 Structures of space–time correlation of bursting phenomena in an open-channel flow. *J. Fluid Mech.* **104**, 1–43.

OFFEN, G. R. & KLINE, S. J. 1974 Combined dye-streak and hydrogen-bubble visual observations of a turbulent boundary layer. *J. Fluid. Mech.* **62**, 223–39.

OFFEN, G. R. & KLINE, S. J. 1975 A proposed model of the bursting process in turbulent boundary layers. *J. Fluid Mech.* **70**, 209–228.

OLDAKER, D. K. & TIEDERMAN, W. G. 1977 Spatial structure of the viscous sublayer in drag reducing channel flows. *Phys. Fluids* **20**, 133–44.

PERRY, A. E. & CHONG, M. S. 1982 On the mechanisms of wall turbulence. *J. Fluid Mech*, **119**, 173–217.

PERRY, A. E., LIM, T. T. & TEH, E. W. 1981 A visual study of turbulent spots. *J. Fluid Mech.* **104**, 387–405.

RUNSTADLER, P. W., KLINE, S. J. & REYNOLDS, W. C. 1963 An experimental investigation of the flow structure of the turbulent boundary layer. *Rep.* MD-8. Dept. of Mech. Engng, Stanford University.

SCHWARTZ, S. P. 1981 Investigation of vortical motions in the inner region of a turbulent boundary layer. M.S. thesis, Department of Mechanical Engineering and Mechanics, Lehigh University, Bethlehem, PA.

SMITH, C. R. 1978 Visualization of turbulent boundary layer structure using a moving hydrogen bubble wire probe. *Lehigh Workshop on Coherent Structure in Turbulent Boundary Layers* (ed. C. R. Smith & D. E. Abbott), pp. 48–97.

SMITH, C. R. 1982 Application of high speed videography for study of complex, three-dimensional water flows. *SPIE*, Vol. 348, pp. 345–352. High Speed Photography (San Diego).

SMITH, C. R. 1984 A synthesized model of the near-wall behavior in turbulent boundary layers. *Proc. 8th Symp. on Turbulence* (ed. G. K. Patterson & J. L. Zakin). Department of Chemical Engineering, University of Missouri, Rolla.

SMITH, C. R. & METZLER, S. P. 1983 The characteristics of low-speed streaks in the near-wall region of a turbulent boundary layer. *J. Fluid Mech.* **129**, 27–54.

TOWNSEND, A. A. 1956 *The Structure of Turbulent Shear Flow*, 1st edn. Cambridge University Press.

UTAMI, T. & UENO, T. 1979 Lagrangian and Eularian measurement of large scale turbulence by flow visualizing techniques. In *Flow Visualization* (ed. T. Asanunra), p. 221. Hemisphere.

VAN DOMMELEN, L. L. 1981 Unsteady boundary layer separation. Ph.D. dissertation, Cornell University.

WALLACE, J. M. 1982 On the structure of bounded turbulent shear flow: a personal view. In *Developments in Theoretical and Applied Mechanics, XI* (ed. T. J. Chung & G. R. Karr), pp. 509–521. Department of Mechanical Engineering, University of Alabama in Huntsville.